Quantitative real-time PCR analysis

RNA was isolated using TRIzol reagent (Invitrogen, 15596026). cDNA was prepared using the Superscript III first strand synthesis kit (Invitrogen, 18080-044) according to the manufacturer's protocol. For mtDNA copy number quantification, genomic DNA was prepared. Quantitative real-time PCR was performed using the Fast SYBR Green Master Mix (Applied Biosystems, 4385612). The primers used for gene expression analysis are listed in **Table S1** and those used for mtDNA copy number analysis are listed in **Table S2.**

Measurement of proteasomal activity

Proteasome activities in soleus muscle extracts were measured using a fluorescent substrate, Suc-LLVY-MCA, as described previously.[46]

Statistics

All data are expressed as means ± s.d. Differences between groups were examined for statistical significance using one-way ANOVA, followed by Tukey-Kramer post hoc test or Student *t* test. A P value < 0.05 was considered statistically significant.

Disclosure of Potential Conflicts of Interest

No potential conflicts of interest were disclosed.

Acknowledgments

We thank Drs Pierre Chambon and Noboru Mizushima for providing the HSA-Cre-ER^{T2} transgenic and GFP-LC3 transgenic mice, respectively. This work was supported in part by a Grant-in-Aid for Young Scientists (B) (22700656 to NF), a Grant-in-Aid for Scientific Research (C) (24500868 to NF), a Grant-in-Aid for Scientific Research on Priority Areas (18076005 to MK, TU), a Grant-in-Aid for Scientific Research on Innovative Areas (23111003 (NH), a Grant-in-Aid for the "High-Tech Research Center" Project for Private Universities, a matching fund subsidy (SI, NF, TU, and EK) from the Ministry of Education, Culture, Sports, Science and Technology (MEXT) of Japan, the MEXT-Supported Program for the Scientific Research Foundation at Private Universities, 2011–2012 (NF), a Research Grant from the Takeda Science Foundation (TU) and an Intramural Research Grant (23-5) for Neurological and Psychiatric Disorders of NCNP (EA-H).

Supplemental Materials

Supplemental materials may be found here:
www.landesbioscience.com/journals/autophagy/article/27785

References

1. Jackman RW, Kandarian SC. The molecular basis of skeletal muscle atrophy. Am J Physiol Cell Physiol 2004; 287:C834-43; PMID:15355854; http://dx.doi.org/10.1152/ajpcell.00579.2003
2. Lecker SH, Solomon V, Mitch WE, Goldberg AL. Muscle protein breakdown and the critical role of the ubiquitin-proteasome pathway in normal and disease states. J Nutr 1999; 129(Suppl):227S-37S; PMID:9915905
3. Mammucari C, Milan G, Romanello V, Masiero E, Rudolf R, Del Piccolo P, Burden SJ, Di Lisi R, Sandri C, Zhao J, et al. FoxO3 controls autophagy in skeletal muscle in vivo. Cell Metab 2007; 6:458-71; PMID:18054315; http://dx.doi.org/10.1016/j.cmet.2007.11.001
4. Masiero E, Agatea L, Mammucari C, Blaauw B, Loro E, Komatsu M, Metzger D, Reggiani C, Schiaffino S, Sandri M. Autophagy is required to maintain muscle mass. Cell Metab 2009; 10:507-15; PMID:19945408; http://dx.doi.org/10.1016/j.cmet.2009.10.008
5. Sandri M, Sandri C, Gilbert A, Skurk C, Calabria E, Picard A, Walsh K, Schiaffino S, Lecker SH, Goldberg AL. Foxo transcription factors induce the atrophy-related ubiquitin ligase atrogin-1 and cause skeletal muscle atrophy. Cell 2004; 117:399-412; PMID:15109499; http://dx.doi.org/10.1016/S0092-8674(04)00400-3
6. Zhao J, Brault JJ, Schild A, Cao P, Sandri M, Schiaffino S, Lecker SH, Goldberg AL. FoxO3 coordinately activates protein degradation by the autophagic/lysosomal and proteasomal pathways in atrophying muscle cells. Cell Metab 2007; 6:472-83; PMID:18054316; http://dx.doi.org/10.1016/j.cmet.2007.11.004
7. Ravid T, Hochstrasser M. Diversity of degradation signals in the ubiquitin-proteasome system. Nat Rev Mol Cell Biol 2008; 9:679-90; PMID:18698327; http://dx.doi.org/10.1038/nrm2468
8. Schwartz AL, Ciechanover A. Targeting proteins for destruction by the ubiquitin system: implications for human pathobiology. Annu Rev Pharmacol Toxicol 2009; 49:73-96; PMID:18834306; http://dx.doi.org/10.1146/annurev.pharmtox.051208.165340
9. Mizushima N, Levine B. Autophagy in mammalian development and differentiation. Nat Cell Biol 2010; 12:823-30; PMID:20811354; http://dx.doi.org/10.1038/ncb0910-823
10. Yang Z, Klionsky DJ. Eaten alive: a history of macroautophagy. Nat Cell Biol 2010; 12:814-22; PMID:20811353; http://dx.doi.org/10.1038/ncb0910-814
11. Mizushima N, Yamamoto A, Matsui M, Yoshimori T, Ohsumi Y. In vivo analysis of autophagy in response to nutrient starvation using transgenic mice expressing a fluorescent autophagosome marker. Mol Biol Cell 2004; 15:1101-11; PMID:14699058; http://dx.doi.org/10.1091/mbc.E03-09-0704
12. Quy PN, Kuma A, Pierre P, Mizushima N. Proteasome-dependent activation of mammalian target of rapamycin complex 1 (mTORC1) is essential for autophagy suppression and muscle remodeling following denervation. J Biol Chem 2013; 288:1125-34; PMID:23209294; http://dx.doi.org/10.1074/jbc.M112.399949
13. Hara T, Nakamura K, Matsui M, Yamamoto A, Nakahara Y, Suzuki-Migishima R, Yokoyama M, Mishima K, Saito I, Okano H, et al. Suppression of basal autophagy in neural cells causes neurodegenerative disease in mice. Nature 2006; 441:885-9; PMID:16625204; http://dx.doi.org/10.1038/nature04724
14. Komatsu M, Waguri S, Chiba T, Murata S, Iwata J, Tanida I, Ueno T, Koike M, Uchiyama Y, Kominami E, et al. Loss of autophagy in the central nervous system causes neurodegeneration in mice. Nature 2006; 441:880-4; PMID:16625205; http://dx.doi.org/10.1038/nature04723
15. Komatsu M, Waguri S, Koike M, Sou YS, Ueno T, Hara T, Mizushima N, Iwata J, Ezaki J, Murata S, et al. Homeostatic levels of p62 control cytoplasmic inclusion body formation in autophagy-deficient mice. Cell 2007; 131:1149-63; PMID:18083104; http://dx.doi.org/10.1016/j.cell.2007.10.035
16. Komatsu M, Waguri S, Ueno T, Iwata J, Murata S, Tanida I, Ezaki J, Mizushima N, Ohsumi Y, Uchiyama Y, et al. Impairment of starvation-induced and constitutive autophagy in Atg7-deficient mice. J Cell Biol 2005; 169:425-34; PMID:15866887; http://dx.doi.org/10.1083/jcb.200412022
17. Murphy MP. How mitochondria produce reactive oxygen species. Biochem J 2009; 417:1-13; PMID:19061483; http://dx.doi.org/10.1042/BJ20081386
18. Kitada T, Asakawa S, Hattori N, Matsumine H, Yamamura Y, Minoshima S, Yokochi M, Mizuno Y, Shimizu N. Mutations in the parkin gene cause autosomal recessive juvenile parkinsonism. Nature 1998; 392:605-8; PMID:9560156; http://dx.doi.org/10.1038/33416
19. Narendra D, Tanaka A, Suen DF, Youle RJ. Parkin is recruited selectively to impaired mitochondria and promotes their autophagy. J Cell Biol 2008; 183:795-803; PMID:19029340; http://dx.doi.org/10.1083/jcb.200809125
20. Yoshii SR, Kishi C, Ishihara N, Mizushima N. Parkin mediates proteasome-dependent protein degradation and rupture of the outer mitochondrial membrane. J Biol Chem 2011; 286:19630-40; PMID:21454557; http://dx.doi.org/10.1074/jbc.M110.209338
21. Lokireddy S, Wijesoma IW, Teng S, Bonala S, Gluckman PD, McFarlane C, Sharma M, Kambadur R. The ubiquitin ligase Mul1 induces mitophagy in skeletal muscle in response to muscle-wasting stimuli. Cell Metab 2012; 16:613-24; PMID:23140641; http://dx.doi.org/10.1016/j.cmet.2012.10.005
22. Sato S, Chiba T, Nishiyama S, Kakiuchi T, Tsukada H, Hatano T, Fukuda T, Yasoshima Y, Kai N, Kobayashi K, et al. Decline of striatal dopamine release in parkin-deficient mice shown by ex vivo autoradiography. J Neurosci Res 2006; 84:1350-7; PMID:16941649; http://dx.doi.org/10.1002/jnr.21032
23. Cha GH, Kim S, Park J, Lee E, Kim M, Lee SB, Kim JM, Chung J, Cho KS. Parkin negatively regulates JNK pathway in the dopaminergic neurons of Drosophila. Proc Natl Acad Sci U S A 2005; 102:10345-50; PMID:16002472; http://dx.doi.org/10.1073/pnas.0500346102
24. Greene JC, Whitworth AJ, Kuo I, Andrews LA, Feany MB, Pallanck LJ. Mitochondrial pathology and apoptotic muscle degeneration in Drosophila parkin mutants. Proc Natl Acad Sci U S A 2003; 100:4078-83; PMID:12642658; http://dx.doi.org/10.1073/pnas.0737556100

25. Pesah Y, Pham T, Burgess H, Middlebrooks B, Verstreken P, Zhou Y, Harding M, Bellen H, Mardon G. Drosophila parkin mutants have decreased mass and cell size and increased sensitivity to oxygen radical stress. Development 2004; 131:2183-94; PMID:15073152; http://dx.doi.org/10.1242/dev.01095
26. Bence NF, Sampat RM, Kopito RR. Impairment of the ubiquitin-proteasome system by protein aggregation. Science 2001; 292:1552-5; PMID:11375494; http://dx.doi.org/10.1126/science.292.5521.1552
27. Korolchuk VI, Mansilla A, Menzies FM, Rubinsztein DC. Autophagy inhibition compromises degradation of ubiquitin-proteasome pathway substrates. Mol Cell 2009; 33:517-27; PMID:19250912; http://dx.doi.org/10.1016/j.molcel.2009.01.021
28. Bodine SC, Latres E, Baumhueter S, Lai VK, Nunez L, Clarke BA, Poueymirou WT, Panaro FJ, Na E, Dharmarajan K, et al. Identification of ubiquitin ligases required for skeletal muscle atrophy. Science 2001; 294:1704-8; PMID:11679633; http://dx.doi.org/10.1126/science.1065874
29. Gomes MD, Lecker SH, Jagoe RT, Navon A, Goldberg AL. Atrogin-1, a muscle-specific F-box protein highly expressed during muscle atrophy. Proc Natl Acad Sci U S A 2001; 98:14440-5; PMID:11717410; http://dx.doi.org/10.1073/pnas.251541198
30. Arlt A, Bauer I, Schafmayer C, Tepel J, Müerköster SS, Brosch M, Röder C, Kalthoff H, Hampe J, Moyer MP, et al. Increased proteasome subunit protein expression and proteasome activity in colon cancer relate to an enhanced activation of nuclear factor E2-related factor 2 (Nrf2). Oncogene 2009; 28:3983-96; PMID:19734940; http://dx.doi.org/10.1038/onc.2009.264
31. Kwak MK, Wakabayashi N, Greenlaw JL, Yamamoto M, Kensler TW. Antioxidants enhance mammalian proteasome expression through the Keap1-Nrf2 signaling pathway. Mol Cell Biol 2003; 23:8786-94; PMID:14612418; http://dx.doi.org/10.1128/MCB.23.23.8786-8794.2003
32. Radhakrishnan SK, Lee CS, Young P, Beskow A, Chan JY, Deshaies RJ. Transcription factor Nrf1 mediates the proteasome recovery pathway after proteasome inhibition in mammalian cells. Mol Cell 2010; 38:17-28; PMID:20385086; http://dx.doi.org/10.1016/j.molcel.2010.02.029
33. Steffen J, Seeger M, Koch A, Krüger E. Proteasomal degradation is transcriptionally controlled by TCF11 via an ERAD-dependent feedback loop. Mol Cell 2010; 40:147-58; PMID:20932482; http://dx.doi.org/10.1016/j.molcel.2010.09.012
34. Biswas M, Chan JY. Role of Nrf1 in antioxidant response element-mediated gene expression and beyond. Toxicol Appl Pharmacol 2010; 244:16-20; PMID:19665035; http://dx.doi.org/10.1016/j.taap.2009.07.034
35. Wang W, Chan JY. Nrf1 is targeted to the endoplasmic reticulum membrane by an N-terminal transmembrane domain. Inhibition of nuclear translocation and transacting function. J Biol Chem 2006; 281:19676-87; PMID:16687406; http://dx.doi.org/10.1074/jbc.M602802200
36. Zhang Y, Lucocq JM, Hayes JD. The Nrf1 CNC/bZIP protein is a nuclear envelope-bound transcription factor that is activated by t-butyl hydroquinone but not by endoplasmic reticulum stressors. Biochem J 2009; 418:293-310; PMID:18990090; http://dx.doi.org/10.1042/BJ20081575
37. Powers SK, Wiggs MP, Duarte JA, Zergeroglu AM, Demirel HA. Mitochondrial signaling contributes to disuse muscle atrophy. Am J Physiol Endocrinol Metab 2012; 303:E31-9; PMID:22395111; http://dx.doi.org/10.1152/ajpendo.00609.2011
38. Zhang Y, Lucocq JM, Yamamoto M, Hayes JD. The NHB1 (N-terminal homology box 1) sequence in transcription factor Nrf1 is required to anchor it to the endoplasmic reticulum and also to enable its asparagine-glycosylation. Biochem J 2007; 408:161-72; PMID:17705787; http://dx.doi.org/10.1042/BJ20070761
39. Cullinan SB, Gordan JD, Jin J, Harper JW, Diehl JA. The Keap1-BTB protein is an adaptor that bridges Nrf2 to a Cul3-based E3 ligase: oxidative stress sensing by a Cul3-Keap1 ligase. Mol Cell Biol 2004; 24:8477-86; PMID:15367669; http://dx.doi.org/10.1128/MCB.24.19.8477-8486.2004
40. Furukawa M, Xiong Y. BTB protein Keap1 targets antioxidant transcription factor Nrf2 for ubiquitination by the Cullin 3-Roc1 ligase. Mol Cell Biol 2005; 25:162-71; PMID:15601839; http://dx.doi.org/10.1128/MCB.25.1.162-171.2005
41. Kobayashi A, Kang MI, Okawa H, Ohtsuji M, Zenke Y, Chiba T, Igarashi K, Yamamoto M. Oxidative stress sensor Keap1 functions as an adaptor for Cul3-based E3 ligase to regulate proteasomal degradation of Nrf2. Mol Cell Biol 2004; 24:7130-9; PMID:15282312; http://dx.doi.org/10.1128/MCB.24.16.7130-7139.2004
42. Zhang DD, Lo SC, Cross JV, Templeton DJ, Hannink M. Keap1 is a redox-regulated substrate adaptor protein for a Cul3-dependent ubiquitin ligase complex. Mol Cell Biol 2004; 24:10941-53; PMID:15572695; http://dx.doi.org/10.1128/MCB.24.24.10941-10953.2004
43. Hayes JD, McMahon M. NRF2 and KEAP1 mutations: permanent activation of an adaptive response in cancer. Trends Biochem Sci 2009; 34:176-88; PMID:19321346; http://dx.doi.org/10.1016/j.tibs.2008.12.008
44. Motohashi H, Yamamoto M. Nrf2-Keap1 defines a physiologically important stress response mechanism. Trends Mol Med 2004; 10:549-57; PMID:15519281; http://dx.doi.org/10.1016/j.molmed.2004.09.003
45. Villeneuve NF, Lau A, Zhang DD. Regulation of the Nrf2-Keap1 antioxidant response by the ubiquitin proteasome system: an insight into cullin-ring ubiquitin ligases. Antioxid Redox Signal 2010; 13:1699-712; PMID:20486766; http://dx.doi.org/10.1089/ars.2010.3211
46. Tanahashi N, Murakami Y, Minami Y, Shimbara N, Hendil KB, Tanaka K. Hybrid proteasomes. Induction by interferon-gamma and contribution to ATP-dependent proteolysis. J Biol Chem 2000; 275:14336-45; PMID:10799514; http://dx.doi.org/10.1074/jbc.275.19.14336

Physiological Reports

Open Access

Physiological Reports ISSN 2051-817X

ORIGINAL RESEARCH

Perlecan deficiency causes endothelial dysfunction by reducing the expression of endothelial nitric oxide synthase

Risa Nonaka[1], Takafumi Iesaki[2], Susana de Vega[1], Hiroyuki Daida[3], Takao Okada[2], Takako Sasaki[4] & Eri Arikawa-Hirasawa[1]

1 Research Institute for Disease of Old Age, Juntendo University Graduate School of Medicine, Tokyo, Japan
2 Department of Physiology, Juntendo University Graduate School of Medicine, Tokyo, Japan
3 Department of Cardiovascular Medicine, Juntendo University Graduate School of Medicine, Tokyo, Japan
4 Department of Biochemistry, Faculty of Medicine, Oita University, Oita, Japan

Keywords
Endothelial cell, nitric oxide synthase, perlecan.

Correspondence
Eri Arikawa-Hirasawa, Juntendo University Graduate School of Medicine, Research Institute for Diseases of Old Age, 2-1-1 Hongo, Bunkyo-ku, Tokyo 113-8421, Japan.
Tel: +81-3-3814-3016
Fax: +81-3-3814-3016
E-mail: ehirasaw@juntendo.ac.jp

Funding Information
This work was supported by a Grant-in-Aid for Young Scientists (B) (24790783) to R.N. and a Grants-in-Aids from the Ministry of Education, Culture, Sports, Science and Technology as well as the Ministry of Health, Labor and Welfare of Japan, Grant for Neurological and Psychiatric Disorders of NCNP (26-8) to E A-H. This study was supported by Grants from MEXT-Supported Program for the Strategic Research Foundation at Private Universities (2011–2015).

Received: 8 October 2014; Revised: 16 December 2014; Accepted: 17 December 2014

doi: 10.14814/phy2.12272

Physiol Rep, 3 (1), 2015, e12272, doi: 10.14814/phy2.12272

Risa Nonaka and Takafumi Iesaki have contributed equally to this work.

Abstract

Perlecan is a major heparan sulfate proteoglycan found in the subendothelial extracellular matrix of the vascular wall. The aim of this study was to investigate the role of perlecan in the regulation of vascular tone. A previously developed conditional perlecan-deficient mouse model was used to measure changes in the isometric force of isolated aortic rings. The vessels were first precontracted with phenylephrine, and then treated with increasing concentrations of vasorelaxants. Endothelium-dependent relaxation, elicited by acetylcholine, was significantly reduced in the perlecan-deficient aortas, whereas endothelium-independent relaxation caused by the exogenous nitric oxide donor sodium nitroprusside remained well preserved. The expression of the endothelial nitric oxide synthase (eNOS) gene, detected by real-time polymerase chain reaction, was significantly decreased in the perlecan-deficient aortas. The expression of eNOS protein detected using Western blotting was also significantly decreased in the perlecan-deficient aortas. We examined the role of perlecan in eNOS gene expression by creating perlecan knockdown human aortic endothelial cells using small interfering RNA (siRNA) for perlecan. Perlecan gene expression was significantly reduced in the perlecan siRNA-treated cells, resulting in a significant decrease in eNOS gene expression. Perlecan deficiency induced endothelial dysfunction, as indicated by a reduction in endothelium-dependent relaxation due, at least partly, to a reduction in eNOS expression. These findings suggest that perlecan plays a role in the activation of eNOS gene expression during normal growth processes.

Introduction

Vascular endothelial cells and vascular smooth muscle cells are two major research targets in the field of vascular physiology. The extracellular matrix in the vascular wall has recently attracted attention, as it not only provides structural support, but also modulates several cellular functions, including cellular adhesion, proliferation,

differentiation, and development (Pillarisetti 2000; Jiang and Couchman 2003; Iozzo 2005). The basement membrane is a thin sheet of the extracellular matrix that underlies the vascular endothelium and surrounds smooth muscle cells. Some of the key constituents of the subendothelial extracellular matrix are heparan sulfate proteoglycans (HSPGs). Perlecan (HSPG2) is a major HSPG in the basement membrane, with a molecular weight of over 400 kDa and a protein core consisting of five domains. It interacts with a number of extracellular matrix molecules, including laminin, collagen IV, fibronectin, fibrillin, and several growth factors, such as vascular endothelial growth factor (VEGF), fibroblast growth factors (FGFs), and platelet-derived growth factor (PDGF) (Iozzo 2005). Perlecan also interacts with plasma lipoprotein very low density lipoprotein (VLDL) (Hummel et al. 2004) and integrin cell surface receptor (Hummel et al. 2004). It also plays a role in a number of processes in the vasculature, including atherosclerosis, tumor angiogenesis, smooth muscle cell activity modulation, endothelial proliferation, and vascular development (Segev et al. 2004).

Others and we have previously reported that the homozygous deletion of *HSPG2* ($HSPG2^{-/-}$) in mice results in lethal chondrodysplasia and in cardiovascular abnormalities, such as transposition of the great arteries (Arikawa-Hirasawa et al. 1999; Costell et al. 1999, 2002). Perlecan deficiency ($HSPG2^{-/-}$) also causes perinatal lethal chondrodysplasia in humans (Costell et al. 1999; Arikawa-Hirasawa et al. 2001), suggesting a crucial role for perlecan in the development of cartilage and in the cardiovascular system. Mutations in the perlecan gene (*HSPG2*) have been identified in patients with Schwartz–Jampel syndrome, a nonlethal condition characterized by myotonia and mild chondrodysplasia (Nicole et al. 2000; Arikawa-Hirasawa et al. 2002; Stum et al. 2006). We investigated the role of perlecan in adult organs using a lethality rescued perlecan-null mouse model expressing recombinant perlecan specifically in cartilage ($HSPG2^{-/-}$-*Tg*) (Xu et al. 2010; Inomata et al. 2012; Ishijima et al. 2012; Kaneko et al. 2013). In addition to our lethality rescued $HSPG2^{-/-}$-*Tg* mouse model, studies employing mutant mice, such as heterozygous perlecan knockout ($HSPG2^{+/-}$) mice (Vikramadithyan et al. 2004) or heparan sulfate (HS)-deficient perlecan expressing mice (Tran-Lundmark et al. 2008), have provided further insights into the in vivo function of perlecan in adult tissues.

Endothelial dysfunction is considered to be a key variable in the pathogenesis of atherosclerosis and in its complications (Bonetti et al. 2002). The dysfunctional condition includes reduction in nitric oxide (NO) bioavailability, which may result in reduced vasorelaxation, thrombus formation, deposition of serum lipids, and the migration and proliferation of vascular smooth muscle cells (VSMCs), which leads to the formation of stenotic lesions in blood vessels (Cai and Harrison 2000). The regulation of vascular tone is the most widely studied aspect of the endothelial function, and NO is the major contributor to endothelium-dependent relaxation in large arteries. In the present study, we investigated the effects of perlecan deletion on endothelium-dependent vascular relaxation during the normal growth process and explored the mechanisms underlying the effects.

Materials and Methods

Animals

Perlecan-null ($HSPG2^{-/-}$) mice die perinatally due to premature cartilage development (Arikawa-Hirasawa et al. 1999; Costell et al. 1999). We previously created a perlecan transgenic mouse line (WT-Tg, $HSPG2^{+/+}$; *COL2A1-*$HSPG2^{Tg/-}$), which expresses recombinant perlecan in cartilage, using a cartilage-specific *COL2A1* promoter/enhancer (Tsumaki et al. 1999) to restore cartilage abnormalities. Subsequently, we created lethality-rescued mice ($HSPG2^{-/-}$ -Tg, $HSPG2^{-/-}$;*COL2A1-*$HSPG2^{Tg/-}$), by mating the transgenic mice with heterozygous $HSPG2^{+/-}$ mice (Xu et al. 2010). We maintained these mice on a mixed genetic background of C57BL/6 and 129SvJ. In the present study, we used $HSPG2^{-/-}$ -Tg mice for the experimental group and WT-Tg ($HSPG2^{+/+}$; *COL2A1-*$HSPG2^{Tg/-}$), mice (10 weeks of age) for the control group. All experimental procedures were performed in accordance with the guidelines for the care and use of animals at Juntendo University, Tokyo, Japan.

Measurement of changes in force in the mice aorta

The mice were sacrificed under anesthesia (Pentobarbital; 50 mg/kg, intraperitoneal administration). The descending thoracic aorta was isolated and cut into transverse rings (~2 mm in length), which were used to measure the changes in force. Care was taken not to touch the endothelial surface in order to preserve the functional endothelium. The techniques used to measure the changes in force were adapted from previously described methods (Iesaki et al. 1999; Sumiyoshi et al. 2008). Briefly, aortic rings were mounted on wire hooks attached to force displacement transducers (Nihon Kohden, Tokyo, Japan) and changes in the isometric force were recorded on a thermal recorder (Rika Denki, Tokyo, Japan). The rings were incubated in individually thermostated (37°C)

10-mL baths filled with oxygenated Krebs bicarbonate buffer (118 mmol/L NaCl, 4.7 mmol/L KCl, 1.5 mmol/L $CaCl_2$, 25 mmol/L $NaHCO_3$, 1.1 mmol/L $MgSO_4$, 1.2 mmol/L KH_2PO_4, and 5.6 mmol/L glucose at pH 7.4). An optimal passive tension of 0.5 g was applied to the rings throughout the experiment. The vascular rings were initially exposed to high-K^+ Krebs bicarbonate buffer, containing 60 mmol/L KCl in place of NaCl to produce maximal force and to enhance the reproducibility of subsequent contractions. After a wash out of high-K^+ buffer, the vessels were submaximally contracted with 1 μmol/L phenylephrine. Once a steady-state level of contraction was achieved, endothelial-dependent relaxation and endothelial-independent relaxation were elicited by the administration of increasing concentrations of acetylcholine (ACh) and sodium nitroprusside (SNP), respectively. Relaxation was expressed as the percent change in the steady-state level of contraction. Comparisons between groups were made with two-way reported measure ANOVA.

Quantitative real-time polymerase chain reaction

Total RNA was isolated from mouse thoracic aortic tissue or human aortic endothelial cells (HAECs; LONZA, Walkersville, MD) using TRIzol reagent (Life Technologies, Carlsbad, CA), according to the manufacturer's instructions. cDNA was generated from 1 μg of total RNA with M-MLV reverse transcriptase (Promega, Madison, WI) and a random primer (TAKARA, Siga, Japan). SYBR Green was used for detection, and RNA expression was normalized to that of the housekeeping gene β-actin for mouse, GAPDH for human. In the graph, the eNOS, von Willebrand factor, and perlecan (HSPG2) expression levels are indicated as relative to β-actin or GAPDH. The PCR reaction was carried out in an ABI Prism® 7500 Fast Sequence Detection System (Life Technologies). The primer sequences were as follows: For the mouse tissue, mouse eNOS forward 5′-CTGGCAGCCCAAGACCTA-3′, mouse eNOS reverse 5′-GTGACATCGCCGCAGACAA-3′, mouse von Willebrand factor forward 5′-GATGCCCCAGTCAGCTCTAC-3′, mouse von Willebrand factor reverse 5′- TCAGCCTCGGACAACATAGA-3′, mouse β-actin forward 5′-TGGAATCCTGTGGCATCCATGAAAC-3′, mouse β-actin reverse 5′-TAAAACGCAGCTCAGTAACAGTCCG-3′. For the HAECs, human HSPG2 forward 5′-GGCTGAGGGCATACGATGGCT-3′, human HSPG2 reverse 5′-CCCACTGCCCAGGTCGTCTCC-3′, human eNOS forward 5′-CCCTTCAGTGGCTGGTACAT-3′, human eNOS reverse 5′-CACGATGGTGACTTTGGCTA-3′, human GAPDH forward 5′-ACCACAGTCCATGCCATCAC-3′, human GAPDH reverse 5′-TCCACCACCCTGTTGCTGTA-3′

Western blotting

Thoracic aortic tissue was isolated and then homogenized in cold lysis buffer, and the lysate was centrifuged at 16,000 *g* for 15 min at 4°C. The lysis buffer contained 50 mmol/L Tris-HCl (pH 7.2), 150 mmol/L NaCl, 1% Nonidet P-40, 1% sodium deoxycholate, 0.1% SDS containing protease, and phosphatase inhibitor cocktails (Complete Protease Inhibitor Cocktail and PhosSTOP; Roche, Rotkreuz, Switzerland). The protein concentration was determined using a BCA protein assay kit (Thermo Scientific, Rockford, IL) and then solubilized in NuPAGE® LDS sample buffer (Life Technologies) containing dithiothreitol. The samples (15 μg/lane) were resolved via electrophoresis on 4–12% SDS-PAGE gels, and then transferred to a PVDF membrane (Life Technologies, Carlsbad, CA). After blocking with PVDF blocking reagent (TOYOBO, Osaka, Japan), the membrane was incubated with primary antibodies in blocking reagent overnight. After washing, the membrane was incubated with horseradish peroxidase (HRP)-conjugated secondary antibodies in blocking reagent and visualized with SuperSignal®West Dura Extended Duration Substrate (Thermo Scientific, Rockford, IL). Specific bands were quantitated using the ImageJ software program. In the graph, the eNOS protein level is indicated as relative to β-actin. The experiments were performed at least three times using different sibling pairs of animals. The antibodies were prepared as follows: the primary antibodies, mouse anti-eNOS/NOS type III antibodies (BD Biosciences, Franklin Lakes, NJ) or mouse anti-β-actin antibody (Santa Cruz Biotechnology, Inc., Dallas, TX) were diluted at 1:1000 or 1:5000 in blocking reagent. The secondary antibodies, anti-mouse IgG HRP-conjugated secondary antibodies (GE Healthcare, Little Chalfont, UK) were diluted at 1:5000 in blocking solution.

Cell culture and small interfering RNA (siRNA)

Human aortic endothelial cells (HAECs) were grown using the Endothelial Cell Growth Media Kit (EGM-2 BulletKit; LONZA), and plated at a density of 2×10^5 cells on 6-well plates. Perlecan siRNA and control siRNA were purchased from Santa Cruz Biotechnology. HAECs were transfected with either perlecan or control siRNA, according to the manufacturer's recommendations. Forty-eight hours after transfection, knockdown efficiency was assessed using quantitative RT-PCR (qPCR), as described above. For perlecan rescue experiments, we used the recombinant perlecan protein (rPerlecan) kindly provided by Dr. Sasaki. The recombinant perlecan was purified from the condition media of 293

cells transfected with a perlecan cDNA expression vector (Noonan et al. 1991; Costell et al. 1997; Xu et al. 2010). The full-length perlecan cDNA (Ishijima et al. 2012) was cloned into the PCEP4-Mul-PURD expression vector (Hozumi et al. 2006), which contains sequences for the CMV promoter, multiple cloning sites, BM40 signal peptide (Hozumi et al. 2006). A twenty-four well tissue culture plate was coated with rPerlecan (20 μg/mL) in PBS, including 1 mmol/L $CaCl_2$ and 0.5 mmol/L $MgCl_2$ at 4°C for 48 h. After the plate was washed twice with PBS, HAECs treated with Perlecan siRNA or Control siRNA, as described above, were plated at density of 3×10^5 cells on the Perlecan or a control plate and cultured for 36 h. The eNOS RNA expression was analyzed using qPCR.

Heparinase III digestion of HAECs

Cell surface heparan sulfate chains of HAECs were digested by heparinase III as described method (Kerever et al. 2007) with some modifications. HAECs were incubated with 5 mU/mL of heparinase III (Sigma-Aldrich, St. Louis, MO) in 50 mmol/L HEPES buffer (pH 7.0), containing 100 mmol/L NaCl and 1 mmol/L $CaCl_2$ at 37°C for 1 h. After the incubation, the heparinase III solution was removed and the cells were cultured with the growth media. We confirmed successful heparinase III digestion using immunostaining. A time course of the eNOS RNA expression was performed using qPCR as described above.

Immunostaining

HAECs were plated at density of 3×10^5 cells on Type-1 collagen-coated 8 well chambers and cultured for 48 h. After heparinase III digestion for 1 h, the cells were fixed immediately (time point 0) or 24 h later (time point 24 h) with 4% paraformaldehyde at room temperature. Nonspecific binding was blocked with 0.2% gelatin/PBS for 10 min and cells were incubated with anti-heparan sulfate antibody (10E4 epitope) antibody or anti-Δheparan sulfate (3G10 epitope) antibody (Seikagaku Corporation, Tokyo, Japan) at 1:400, and anti-perlecan (clone A7L6) (Chemicon, Temecula, CA) antibody at 1:400 in 0.2% gelatin/PBS at 4°C overnight. Following a wash with PBS, the cells were incubated with goat anti-mouse IgM alexafluor 488 and goat anti-rat IgG alexafluor 546 (Molecular Probes, Invitrogen Corporation, Carlsbad, CA) at 1:400 in 0.2% gelatin/PBS for 1 h. The cells were washed and then incubated for 10 min in bis-benzimide (1:5000, Molecular Probes, Invitrogen Corporation). After extensive washes, cells were mounted in fluoro-gel with Tris buffer (Electron Microscopy Sciences, Hatfield, PA). Images were taken using a Leica TCS-SP5 LSM confocal microscope.

Statistical analysis

The data are presented as the mean ± SEM. Comparisons between groups were made with two-way reported measure ANOVA and with the unpaired *t*-test. A *P* value of <0.05 was considered to be statistically significant.

Results

HSPG2 deletion decreases the relaxation of mouse aorta

An endothelium-dependent relaxation of the mouse aorta was elicited by ACh. Aortic relaxation in response to ACh was significantly reduced in the *HSPG2*$^{-/-}$-Tg aortas compared to that of the control aortas, resulting in the downward shift of the concentration-response curve (Fig. 1A). On the other hand, the endothelium-independent relaxation elicited by exogenous nitric oxide donor

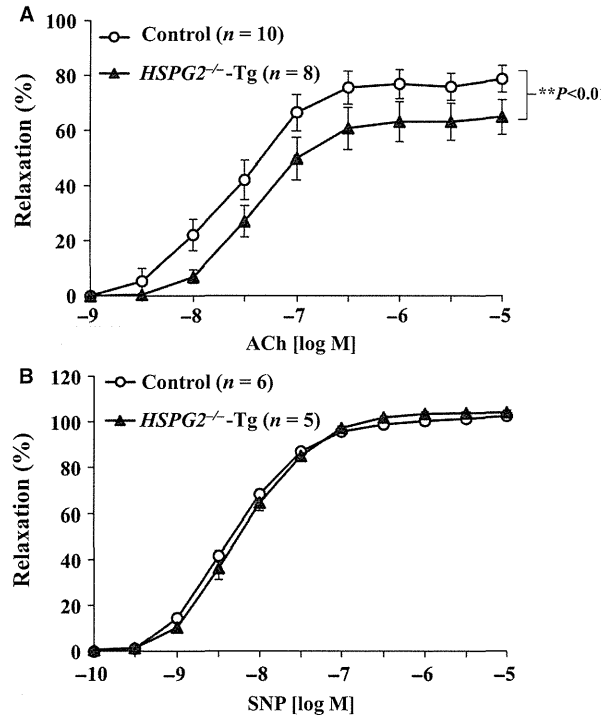

Figure 1. *HSPG2*$^{-/-}$-Tg aortas have a reduced relaxation in response to ACh or SNP. The aortic rings were precontracted with 1 μmol/L phenylephrine (PE), and increasing concentrations of (A) acetylcholine (ACh) or (B) sodium nitroprusside (SNP) were added. The degree of relaxation is expressed as the percent relaxation of the PE-induced tone (The bars indicate the mean ± SEM, *n* = 5–10).

SNP was not affected by the deletion of *HSPG2*, as shown in Figure 1B, indicating that the sensitivity of vascular smooth muscle to exogenous nitric oxide donors is well preserved, even in *HSPG2*$^{-/-}$-Tg aortas.

HSPG2 deletion decreases the expression level of eNOS in mouse aortas

We explored the mechanisms underlying the reduction of endothelium-dependent relaxation by measuring RNA expression levels of both eNOS and von Willebrand factor (vWF), an endothelial cell specific gene, using qPCR. RNA was extracted from aortic tissue from control and from *HSPG2*$^{-/-}$-Tg animals. The vWF expression level in the control and in the *HSPG2*$^{-/-}$-Tg aortas was not significantly different (Fig. 2A). However, qPCR analysis revealed that eNOS mRNA expression was significantly reduced in the *HSPG2*$^{-/-}$-Tg aortas (Fig. 2B). We also measured protein expression levels of eNOS in the control and in the *HSPG2*$^{-/-}$-Tg aortas by Western blotting. The protein level of eNOS was significantly decreased in the *HSPG2*$^{-/-}$-Tg aortas compared with that of the control aortas (Fig. 2C). These results indicated that eNOS expression was decreased in the perlecan-deficient aortas.

eNOS expression was decreased in HAECs by Perlecan siRNA treatment

We examined the relationship between eNOS expression and perlecan expression by creating perlecan knockdown HAECs in culture using Perlecan siRNA treatment. We measured the RNA expression levels by qPCR using RNA extracted from HAECs treated with control or Perlecan siRNA. We confirmed that perlecan mRNA expression levels in HAECs were significantly decreased by approximately 90% following treatment with both 20 and 40 nmol of Perlecan siRNA (Fig. 3A). The eNOS mRNA expression was significantly decreased by approximately 50% following Perlecan siRNA treatment (Fig. 3B). These results indicated that reduced perlecan expression decreases eNOS expression in HAECs.

Depletion of heparan sulfate chains does not affect the eNOS expression

We performed enzymatic depletion of the heparan sulfate chains of perlecan on HAECs to explore whether heparan sulfate chains are critical for eNOS expression. The time course of the experimental protocol is shown in Figure 4A. First, we confirmed the depletion of heparan

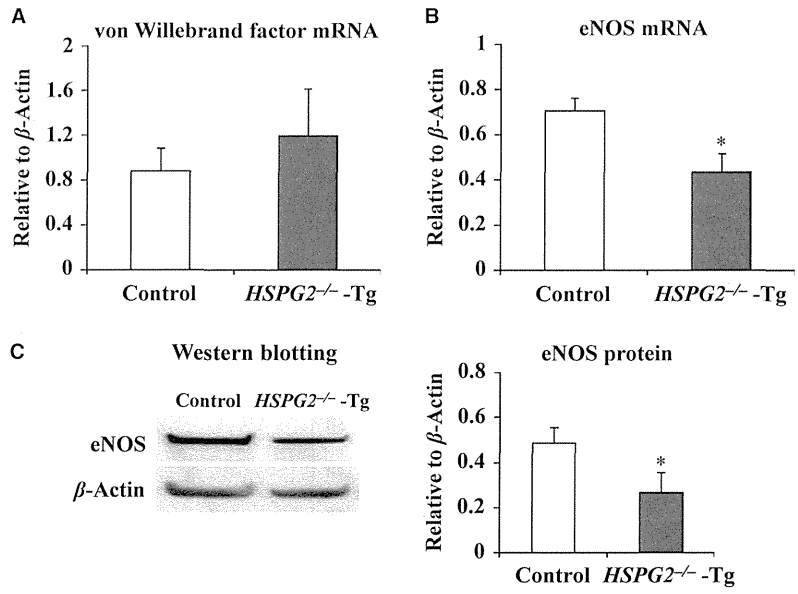

Figure 2. Expression of endothelial nitric oxide synthase (eNOS) in the *HSPG2*$^{-/-}$-Tg aorta. RNA expression levels of von Willebrand factor and eNOS in the aortic tissues of 10 week control and *HSPG2*$^{-/-}$-Tg mice were analyzed using qPCR. (A) The expression of von Willebrand factor was not significantly different, while (B) eNOS expression was significantly reduced in the *HSPG2*$^{-/-}$-Tg animals (n = 6 per genotype. The bars indicate the mean ± SEM). RNA expressions levels were normalized to that of β-actin and were indicated as relative to β-actin. (C) The protein expression levels of eNOS and β-actin in the aortic tissues were evaluated, using Western blotting. Each band was quantified using ImageJ software and is shown as relative to β-actin. The protein expression levels of eNOS were significantly decreased in the HSPG2$^{-/-}$-Tg mice compared to that in the control mice (n = 4 per genotype. The bars indicate the mean ± SEM). *P < 0.05 versus control mice.

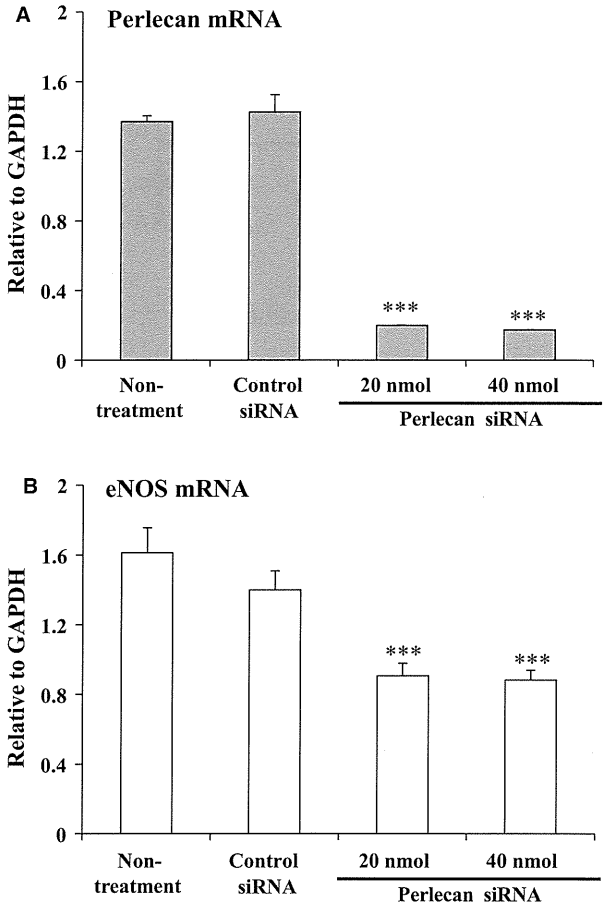

Figure 3. RNA expression of eNOS in human aortic endothelial cells (HAECs) treated with *HSPG2* siRNA. Analyses of perlecan and eNOS RNA expression levels in the HAECs treated with or without control siRNA and 20 or 40 nmol of Perlecan siRNA using qPCR. RNA expressions were normalized to that of GAPDH and are indicated as relative to GAPDH. (A) Perlecan expression in HAECs was significantly decreased by approximately 90% following Perlecan siRNA treatment. (B) eNOS expression showed a significant decrease of approximately 50% following treatment with Perlecan siRNA. The bars indicate the mean ± SEM (n = 3), ***P < 0.001 versus control cells.

sulfate chains in HAECs by immunostaining using 10E4 and 3G10 antibodies. After heparinase III treatment for 1 h (time point 0), the staining by 10E4 antbody (green), which is directed against heparan sulfate chains, was not detected (Fig. 4Ba and Bc) and the staining by 3G10 antibody (green), which is directed against heparinase-generated HS stubs, was detected in the treated but not untreated HAECs (Fig. 4Bb and Bd). Similar results were obtained after 24 h (time point 24 h) (Fig. 4Be–Bh). In these conditions, we analyzed eNOS expression by qPCR at 1, 12, and 24 h after heparinase III treatment for 1 h. The eNOS expression levels in the heparinase treated HAECs were not different compared with that of the non-treated HAECs at any time point (Fig. 4C). These results suggest that the decrease of eNOS expression in perlecan-deficient aortas is not due to the heparan sulfate chains.

Perlecan protein is necessary for eNOS expression

In order to explore whether perlecan protein is critical for eNOS expression, we performed perlecan rescue experiments using recombinant perlecan protein (rPerlecan). HAECs treated with Perlecan siRNA or Control siRNA were seeded on plates coated with or without rPerlecan. After 36 h, the eNOS expression level was analyzed by qPCR. First, we confirmed that the eNOS expression level in HAECs treated with Perlecan siRNA was significantly decreased compared with that of Control siRNA. However, the eNOS expression level in HAECs treated with Perlecan siRNA was restored to the level almost similar to that in HAECs treated with Control siRNA by rPerlecan (Fig. 5). These results suggest that perlecan is responsible for the decrease in eNOS expression in perlecan-deficient aortas.

Discussion

In the present study, we showed that a deficiency of perlecan results in the impairment of endothelium-dependent vascular relaxation in mice aorta, whereas endothelium-independent relaxation in response to the nitric oxide donor SNP remained well preserved. We investigated the mechanism(s) underlying the reduction in endothelium-dependent relaxation by examining the eNOS expression levels in aortic tissue and found that both eNOS mRNA and protein levels were decreased in the perlecan-null aortas. We further examined the relationship between perlecan deficiency and a decreased eNOS expression by treating HAECs with perlecan siRNA and found that a reduction in the perlecan gene expression induced a decrease in eNOS gene expression. This is the first report to show that perlecan deficiency results in a reduction in endothelium-dependent relaxation due, at least partly, to a decrease in eNOS expression. Although perlecan has been implicated in vascular development, the function of VSMCs with respect to relaxation is not affected by the deletion of the perlecan gene, suggesting a lesser contribution of perlecan in VSMCs than in endothelial cells.

NO is a gaseous lipophilic free radical generated by constitutively expressed eNOS in vascular endothelial cells (Braam and Verhaar 2007). The expression levels of eNOS are altered in patients with various pathophysiological

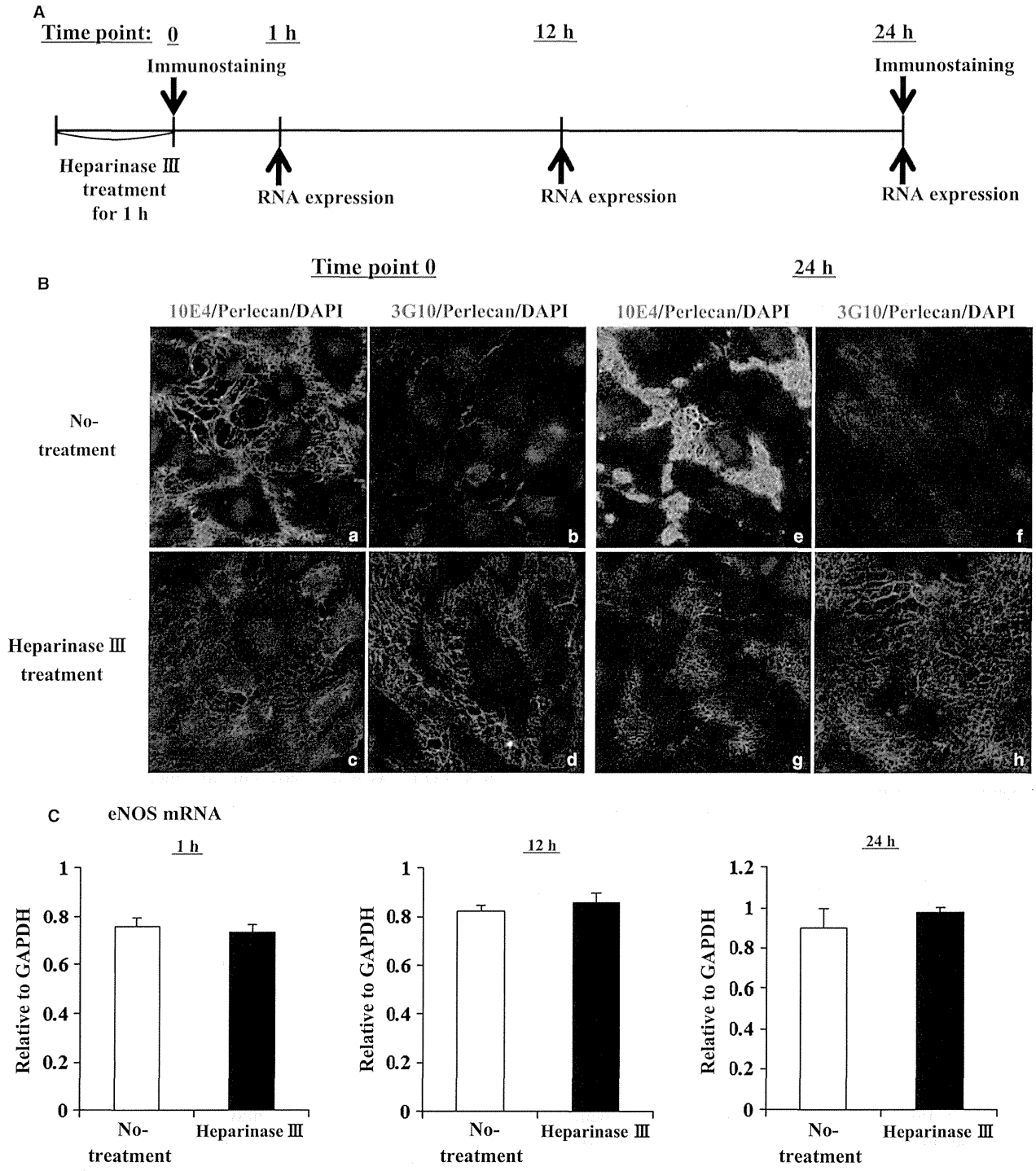

Figure 4. RNA expression levels of eNOS in HAECs treated with heparinase III. (A) A time course of experimental protcol using heparitinase III. (B) The heparan sulfate chains were removed from HAECs using heparinase III. After a 1 h treatment with or without heparinase III, the cells were fixed immediately (time point 0) or 24 h later (time point 24 h), and immunostaining was performed with 10E4 or 3G10 (Green), and perlecan (Red) antibodies. Successful heparinase III digestion is indicated by negative staining of 10E4 (c and g) and positive staining of 3G10 (d and h). At 24 h culture after heparinase III treatment, heparan sulfate chains were not detected (g and h). (C) Analysis of eNOS RNA expression levels in HAECs treated with or without heparinase III using qPCR. eNOS RNA expressions was normalized to that of GAPDH and it is indicated as relative to GAPDH. eNOS expression levels in the heparinase III treated HAECs was not significantly different compared with that of the non-treated HAECs at 1, 12, and 24 h later. The bars indicate the mean ± SEM (n = 3)

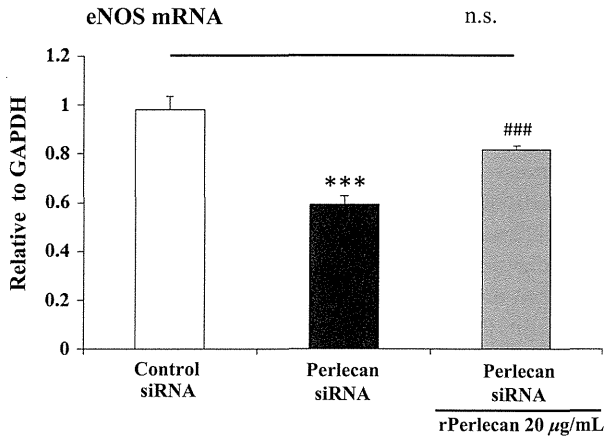

Figure 5. RNA expression level of eNOS in Perlecan knockdown HAECs on perlecan recombinant protein. qPCR analysis of eNOS RNA expression level in HAECs treated with Perlecan or Control siRNA and seeded on a plate coated with or without perlecan recombinant protein (rPerlecan). The level of the eNOS RNA expression was normalized to that of GAPDH and it is indicated as relative to GAPDH. The eNOS expression level in HAECs treated with Perlecan siRNA was significantly decreased compared to that of Control siRNA treated HAECs. HAECs treated with Perlecan siRNA and plated on rPerlecan was no significantly different compared with that of Control siRNA treated HAECs. The bars indicate the mean ± SEM ($n = 4$) $^{***}P < 0.001$ versus Control siRNA treated HAECs without rPerlecan, $^{###}P < 0.001$ versus Perlecan siRNA treated HAECs without rPerlecan.

conditions, such as cardiovascular disease, atherosclerosis, diabetes mellitus, and hypertension (Chatterjee et al. 2008). The transcriptional activation of the eNOS gene is stimulated by shear stress (Papapetropoulos et al. 1999), exercise (Sessa et al. 1994), and the action of lysophosphatidylcholine (Zembowicz et al. 1995) and several growth factors, including VEGF (Bouloumie et al. 1999), bFGF, and epidermal growth factor (EGF) (Braam and Verhaar 2007). Conversely, eNOS expression is down-regulated by tumor necrosis factor-alpha (TNF-α) (Nishida et al. 1992), hypoxia (McQuillan et al. 1994), and high concentrations of low-density lipoprotein (LDL) (Laufs et al. 1998). eNOS activity at the post-translational level is regulated by several mechanisms, including interactions with other proteins, acylation, phosphorylation, and cellular localization (Braam and Verhaar 2007). In the present study, we demonstrated that perlecan plays a role in endothelium-dependent vascular relaxation, acting in part through maintenance of the eNOS expression levels.

Proliferation of endothelial cells requires multiple growth factors, including VEGF and FGF-2 (Carmeliet 2000; Iozzo and San Antonio 2001), which elicit their activities by binding to HSPGs in the vascular wall (Iozzo and San Antonio 2001). These growth factors must bind to HSPGs in the vascular wall in order to function stably (Iozzo and San Antonio 2001). These growth factors also upregulate eNOS expression (Braam and Verhaar 2007), therefore it is conceivable that perlecan deficiency results in reduced binding of growth factors to the vessel wall, thereby reducing eNOS expression. The expression of vWF, another marker of endothelial cells, was not affected by perlecan deficiency in this study, suggesting that the reduction in eNOS expression is rather specific to perlecan deficiency. Perlecan binds to several growth factors, including VEGF and FGF-2, via its HS chains (Zoeller et al. 2009). Perlecan from endothelial cells and the recombinant endorepellin protein, a C-terminal fragment of perlecan, binds to VEGFR-1 and -2, and modulate the VEGF-VEGFR signaling pathway in endothelial cells (Goyal et al. 2011; Ishijima et al. 2012). In this study, we showed that the depletion of heparan sulfate chains did not affect the eNOS expression level in HAECs. On the other hand, the eNOS expression level of HAECs treated with Perlecan siRNA was restored to the similar level of Control siRNA in the presence of recombinant perlecan protein. These results suggest that the decrease in the eNOS expression level in perlecan knockout aorta is due to the deficiency of the perlecan core protein. The precise mechanisms that underlie this reduced eNOS expression induced by perlecan deficiency remain to be elucidated. However, this study is the first, to our knowledge, to show a direct relationship between perlecan deficiency and a reduction in eNOS mRNA expression.

We previously reported that heterozygous deficiency of perlecan results in a reduced rate of atherosclerosis in apoE null mice (Vikramadithyan et al. 2004), suggesting that perlecan possesses pro-atherosclerotic properties. In addition, perlecan heparan sulfate (HS) chains promote atherosclerosis, as the depletion of endogenous perlecan HS was associated with a reduced frequency of atherosclerosis in apoE null mice (Tran-Lundmark et al. 2008), again suggesting that perlecan is pro-atherosclerotic. In contrary, our results suggest that the perlecan protein plays an atheroprotective role by activating the expression of eNOS during the normal growth process. The discrepancy in these results may be due to the differences in the animal models used and the time points of observation in each study, as the formation of atherosclerotic lesions is a chronic process that includes multiple steps of progression over several weeks. In the present study, we examined the role of perlecan in normal growth, not in animals exposed to atherosclerotic stimuli.

We previously investigated the effects of perlecan deletion on several adult organs in mice, including skeletal muscle (Xu et al. 2010), corneal epithelial tissues (Inomata

et al. 2012), endochondral bone formation (Ishijima et al. 2012), and synovial joints in the setting of knee osteoarthritis (Kaneko et al. 2013). Taken together, the results suggested that perlecan plays diverse roles in supporting tissues and homeostasis of tissue functions. In the present study, we found that the deletion of perlecan resulted in endothelial dysfunction, which is a new and rather unexpected finding, despite previous reports indicating that perlecan plays a role in the development of the cardiovascular system (Costell et al. 2002). This finding may indicate a potential cardiovascular risk in patients with Schwartz–Jampel syndrome, a disease caused by mutations in the perlecan gene in humans (Nicole et al. 2000; Arikawa-Hirasawa et al. 2002; Stum et al. 2006).

In conclusion, we showed that deficiency of perlecan led to endothelial dysfunction, as represented by a reduction in endothelium-dependent relaxation, which is thought to constitute the very early phase of atherosclerosis (Vanhoutte 2009). This dysfunction was due, at least partly, to a reduction in eNOS expression, indicating that perlecan plays a role in the activation of eNOS gene expression during normal growth.

Acknowledgments

We specially thank Dr. Y.Yamada for valuable advice, and Dr. Z. Xu, Dr. N. Liang, Dr. A. Kerever, Dr. T. Nakamura, and Dr. K. Sumiyoshi for the mouse management and technical assistance.

Conflict of Interest

None declared.

References

Arikawa-Hirasawa, E., H. Watanabe, H. Takami, J. R. Hassell, and Y. Yamada. 1999. Perlecan is essential for cartilage and cephalic development. Nat. Genet. 23:354–358.

Arikawa-Hirasawa, E., W. R. Wilcox, A. H. Le, N. Silverman, P. Govindraj, J. R. Hassell, et al. 2001. Dyssegmental dysplasia, Silverman-Handmaker type, is caused by functional null mutations of the perlecan gene. Nat. Genet. 27:431–434.

Arikawa-Hirasawa, E., A. H. Le, I. Nishino, I. Nonaka, N. C. Ho, C. A. Francomano, et al. 2002. Structural and functional mutations of the perlecan gene cause Schwartz-Jampel syndrome, with myotonic myopathy and chondrodysplasia. Am. J. Hum. Genet. 70:1368–1375.

Bonetti, P. O., S. H. Wilson, M. Rodriguez-Porcel, D. R. Jr Holmes, L. O. Lerman, and A. Lerman. 2002. Simvastatin preserves myocardial perfusion and coronary microvascular permeability in experimental hypercholesterolemia independent of lipid lowering. J. Am. Coll. Cardiol. 40:546–554.

Bouloumie, A., V. B. Schini-Kerth, and R. Busse. 1999. Vascular endothelial growth factor up-regulates nitric oxide synthase expression in endothelial cells. Cardiovasc. Res. 41:773–780.

Braam, B., and M. C. Verhaar. 2007. Understanding eNOS for pharmacological modulation of endothelial function: a translational view. Curr. Pharm. Des. 13:1727–1740.

Cai, H., and D. G. Harrison. 2000. Endothelial dysfunction in cardiovascular diseases: the role of oxidant stress. Circ. Res. 87:840–844.

Carmeliet, P. 2000. Mechanisms of angiogenesis and arteriogenesis. Nat. Med. 6:389–395.

Chatterjee, A., S. M. Black, and J. D. Catravas. 2008. Endothelial nitric oxide (NO) and its pathophysiologic regulation. Vascul. Pharmacol. 49:134–140.

Costell, M., K. Mann, Y. Yamada, and R. Timpl. 1997. Characterization of recombinant perlecan domain I and its substitution by glycosaminoglycans and oligosaccharides. Eur. J. Biochem. 243:115–121.

Costell, M., E. Gustafsson, A. Aszodi, M. Morgelin, W. Bloch, E. Hunziker, et al. 1999. Perlecan maintains the integrity of cartilage and some basement membranes. J. Cell Biol. 147:1109–1122.

Costell, M., R. Carmona, E. Gustafsson, M. Gonzalez-Iriarte, R. Fassler, and R. Munoz-Chapuli. 2002. Hyperplastic conotruncal endocardial cushions and transposition of great arteries in perlecan-null mice. Circ. Res. 91:158–164.

Goyal, A., N. Pal, M. Concannon, M. Paul, M. Doran, C. Poluzzi, et al. 2011. Endorepellin, the angiostatic module of perlecan, interacts with both the alpha2beta1 integrin and vascular endothelial growth factor receptor 2 (VEGFR2): a dual receptor antagonism. J. Biol. Chem. 286:25947–25962.

Hozumi, K., N. Suzuki, P. K. Nielsen, M. Nomizu, and Y. Yamada. 2006. Laminin alpha1 chain LG4 module promotes cell attachment through syndecans and cell spreading through integrin alpha2beta1. J. Biol. Chem. 281:32929–32940.

Hummel, S., A. Osanger, T. M. Bajari, M. Balasubramani, W. Halfter, J. Nimpf, et al. 2004. Extracellular matrices of the avian ovarian follicle. Molecular characterization of chicken perlecan. J. Biol. Chem. 279:23486–23494.

Iesaki, T., S. A. Gupte, P. M. Kaminski, and M. S. Wolin. 1999. Inhibition of guanylate cyclase stimulation by NO and bovine arterial relaxation to peroxynitrite and H2O2. Am. J. Physiol. 277:H978–H985.

Inomata, T., N. Ebihara, T. Funaki, A. Matsuda, Y. Watanabe, L. Ning, et al. 2012. Perlecan-deficient mutation impairs corneal epithelial structure. Invest. Ophthalmol. Vis. Sci. 53:1277–1284.

Iozzo, R. V. 2005. Basement membrane proteoglycans: from cellar to ceiling. Nat. Rev. Mol. Cell Biol. 6:646–656.

Iozzo, R. V., and J. D. San Antonio. 2001. Heparan sulfate proteoglycans: heavy hitters in the angiogenesis arena. J. Clin. Invest. 108:349–355.

Ishijima, M., N. Suzuki, K. Hozumi, T. Matsunobu, K. Kosaki, H. Kaneko, et al. 2012. Perlecan modulates VEGF signaling and is essential for vascularization in endochondral bone formation. Matrix Biol. 31:234–245.

Jiang, X., and J. R. Couchman. 2003. Perlecan and tumor angiogenesis. J. Histochem. Cytochem. 51:1393–1410.

Kaneko, H., M. Ishijima, I. Futami, N. Tomikawa-Ichikawa, K. Kosaki, R. Sadatsuki, et al. 2013. Synovial perlecan is required for osteophyte formation in knee osteoarthritis. Matrix Biol. 32:178–187.

Kerever, A., J. Schnack, D. Vellinga, N. Ichikawa, C. Moon, E. Arikawa-Hirasawa, et al. 2007. Novel extracellular matrix structures in the neural stem cell niche capture the neurogenic factor fibroblast growth factor 2 from the extracellular milieu. Stem Cells 25:2146–2157.

Laufs, U., V. La Fata, J. Plutzky, and J. K. Liao. 1998. Upregulation of endothelial nitric oxide synthase by HMG CoA reductase inhibitors. Circulation 97:1129–1135.

McQuillan, L. P., G. K. Leung, P. A. Marsden, S. K. Kostyk, and S. Kourembanas. 1994. Hypoxia inhibits expression of eNOS via transcriptional and posttranscriptional mechanisms. Am. J. Physiol. 267:H1921–H1927.

Nicole, S., C. S. Davoine, H. Topaloglu, L. Cattolico, D. Barral, P. Beighton, et al. 2000. Perlecan, the major proteoglycan of basement membranes, is altered in patients with Schwartz-Jampel syndrome (chondrodystrophic myotonia). Nat. Genet. 26:480–483.

Nishida, K., D. G. Harrison, J. P. Navas, A. A. Fisher, S. P. Dockery, M. Uematsu, et al. 1992. Molecular cloning and characterization of the constitutive bovine aortic endothelial cell nitric oxide synthase. J. Clin. Invest. 90:2092–2096.

Noonan, D. M., A. Fulle, P. Valente, S. Cai, E. Horigan, M. Sasaki, et al. 1991. The complete sequence of perlecan, a basement membrane heparan sulfate proteoglycan, reveals extensive similarity with laminin A chain, low density lipoprotein-receptor, and the neural cell adhesion molecule. J. Biol. Chem. 266:22939–22947.

Papapetropoulos, A., R. D. Rudic, and W. C. Sessa. 1999. Molecular control of nitric oxide synthases in the cardiovascular system. Cardiovasc. Res. 43:509–520.

Pillarisetti, S. 2000. Lipoprotein modulation of subendothelial heparan sulfate proteoglycans (perlecan) and atherogenicity. Trends Cardiovasc. Med. 10:60–65.

Segev, A., N. Nili, and B. H. Strauss. 2004. The role of perlecan in arterial injury and angiogenesis. Cardiovasc. Res. 63:603–610.

Sessa, W. C., K. Pritchard, N. Seyedi, J. Wang, and T. H. Hintze. 1994. Chronic exercise in dogs increases coronary vascular nitric oxide production and endothelial cell nitric oxide synthase gene expression. Circ. Res. 74:349–353.

Stum, M., C. S. Davoine, S. Vicart, L. Guillot-Noel, H. Topaloglu, F. J. Carod-Artal, et al. 2006. Spectrum of HSPG2 (Perlecan) mutations in patients with Schwartz-Jampel syndrome. Hum. Mutat. 27:1082–1091.

Sumiyoshi, K., H. Mokuno, T. Iesaki, K. Shimada, T. Miyazaki, A. Kume, et al. 2008. Deletion of the Fc receptors gamma chain preserves endothelial function affected by hypercholesterolaemia in mice fed on a high-fat diet. Cardiovasc. Res. 80:463–470.

Tran-Lundmark, K., P. K. Tran, G. Paulsson-Berne, V. Friden, R. Soininen, K. Tryggvason, et al. 2008. Heparan sulfate in perlecan promotes mouse atherosclerosis: roles in lipid permeability, lipid retention, and smooth muscle cell proliferation. Circ. Res. 103:43–52.

Tsumaki, N., K. Tanaka, E. Arikawa-Hirasawa, T. Nakase, T. Kimura, J. T. Thomas, et al. 1999. Role of CDMP-1 in skeletal morphogenesis: promotion of mesenchymal cell recruitment and chondrocyte differentiation. J. Cell Biol. 144:161–173.

Vanhoutte, P. M. 2009. Endothelial dysfunction: the first step toward coronary arteriosclerosis. Circ. J. 73:595–601.

Vikramadithyan, R. K., Y. Kako, G. Chen, Y. Hu, E. Arikawa-Hirasawa, Y. Yamada, et al. 2004. Atherosclerosis in perlecan heterozygous mice. J. Lipid Res. 45:1806–1812.

Xu, Z., N. Ichikawa, K. Kosaki, Y. Yamada, T. Sasaki, L. Y. Sakai, et al. 2010. Perlecan deficiency causes muscle hypertrophy, a decrease in myostatin expression, and changes in muscle fiber composition. Matrix Biol. 29:461–470.

Zembowicz, A., J. L. Tang, and K. K. Wu. 1995. Transcriptional induction of endothelial nitric oxide synthase type III by lysophosphatidylcholine. J. Biol. Chem. 270:17006–17010.

Zoeller, J. J., J. M. Whitelock, and R. V. Iozzo. 2009. Perlecan regulates developmental angiogenesis by modulating the VEGF-VEGFR2 axis. Matrix Biol. 28:284–291.

Available online at www.sciencedirect.com

ScienceDirect

Neuromuscular Disorders 25 (2015) 60–69

www.elsevier.com/locate/nmd

Congenital myasthenic syndrome in Japan: Ethnically unique mutations in muscle nicotinic acetylcholine receptor subunits

Yoshiteru Azuma [a,b], Tomohiko Nakata [a,b], Motoki Tanaka [c], Xin-Ming Shen [d], Mikako Ito [a], Satoshi Iwata [a], Tatsuya Okuno [a], Yoshiko Nomura [e], Naoki Ando [f], Keiko Ishigaki [g], Bisei Ohkawara [a], Akio Masuda [a], Jun Natsume [b], Seiji Kojima [b], Masahiro Sokabe [c], Kinji Ohno [a,*]

[a] *Division of Neurogenetics, Center for Neurological Diseases and Cancer, Nagoya University Graduate School of Medicine, Nagoya, Japan*
[b] *Department of Pediatrics, Nagoya University Graduate School of Medicine, Nagoya, Japan*
[c] *Department of Physiology, Nagoya University Graduate School of Medicine, Nagoya, Japan*
[d] *Department of Neurology, Mayo Clinic, Rochester, MN, USA*
[e] *Segawa Neurological Clinic for Children, Tokyo, Japan*
[f] *Department of Pediatrics, Nagoya City University Graduate School of Medicine, Nagoya, Japan*
[g] *Department of Pediatrics, Tokyo Women's Medical University, Tokyo, Japan*

Received 29 May 2014; received in revised form 9 August 2014; accepted 3 September 2014

Abstract

Congenital myasthenic syndromes (CMS) are caused by mutations in genes expressed at the neuromuscular junction. Most CMS patients have been reported in Western and Middle Eastern countries, and only four patients with *COLQ* mutations have been reported in Japan. We here report six mutations in acetylcholine receptor (AChR) subunit genes in five Japanese patients. Five mutations are novel, and one mutation is shared with a European American patient but with a different haplotype. Among the observed mutations, p.Thr284Pro (p.Thr264Pro according to the legacy annotation) in the epsilon subunit causes a slow-channel CMS. Five other mutations in the delta and epsilon subunits are splice site, frameshift, null, or missense mutations causing endplate AChR deficiency. We also found a heteroallelic p.Met465Thr in the beta subunit in another patient. p.Met465Thr, however, was likely to be polymorphism, because single channel recordings showed mild shortening of channel openings without affecting cell surface expression of AChR, and the minor allelic frequency of p.Met465Thr was 5.1% in the Japanese population. Lack of shared mutant alleles between the Japanese and the other patients suggests that most mutations described here are ethnically unique or *de novo* in each family.

Keywords: Congenital myasthenic syndromes; Acetylcholine receptor; Slow channel syndrome; Fast channel syndrome; Endplate acetylcholine receptor deficiency

1. Introduction

Acetylcholine released from the nerve terminal binds to muscle nicotinic acetylcholine receptor (AChR) at the motor endplate. AChR is clustered at the neuromuscular junction (NMJ) by binding to rapsyn with a stoichiometry of rapsyn to AChR of 1:1 to 2:1 [1]. AChR clustering is mediated by neural agrin that is released from the nerve terminal [2]. In early embryonic development, AChR clustering is also mediated by Wnt ligands [3,4]. Embryonic AChR is composed of α, β, δ, and γ subunits with a stoichiometry of $\alpha_2\beta\delta\gamma$. After birth, the ε subunit is substituted for the γ subunit, generating $\alpha_2\beta\delta\varepsilon$-AChR.

Congenital myasthenic syndromes (CMS) are heterogeneous disorders caused by mutations in genes expressed at the NMJ [5]. They are characterized by fatigable muscle weakness, variable muscle atrophy, and sometimes dysmorphic features. CMS mutations have been reported in 19 genes, with most mutations in *CHRNA1*, *CHRNB1*, *CHNRD*, and *CHNRE* encoding the AChR α, β, δ, and ε subunits, respectively. These mutations fall into three subsets: i) slow-channel CMS (SCCMS), in which the open time of AChR is abnormally prolonged; ii) fast-channel CMS (FCCMS), in which the open time of AChR is abnormally brief; and iii) endplate AChR deficiency. SCCMS is caused by a gain-of-function mutation and is dominantly inherited with variable penetrance [6]. In contrast, FCCMS and endplate AChR deficiency are caused by loss-of-function mutations on both alleles, and are recessively

* Corresponding author. Division of Neurogenetics, Center for Neurological Disease and Cancer, Nagoya University Graduate School of Medicine, 65 Tsurumai, Showa-ku, Nagoya 466-8550, Japan. Tel.: +81 52 744 2446; fax: +81 52 744 2449.
E-mail address: ohnok@med.nagoya-u.ac.jp (K. Ohno).

http://dx.doi.org/10.1016/j.nmd.2014.09.002
0960-8966/

inherited. Low-expressor mutations of the AChR ε subunit are partly compensated for by expression of the embryonic AChR γ subunit, whereas the other AChR subunits have no substituting subunits. Accordingly, null and frameshift mutations are frequently detected in *CHRNE*, but not in the other subunit genes.

More than 500 patients with CMS have been reported in Western and Middle Eastern countries, whereas only four Japanese CMS patients carrying five mutations in *COLQ* encoding collagen Q that anchors acetylcholinesterase (AChE) at the NMJ have been reported by us [7,8]. Among the more than 450 CMS mutations in 19 disease genes registered in the Human Gene Mutation Database (http://www.hgmd.org), two likely have founder effects: p.Asn88Lys in *RAPSN* [9–11] and c.1124_1127dupTGCC in *DOK7* [12], whereas the others are private mutations occurring in a single or a small number of unrelated families. We here report five Japanese CMS patients with six mutations in the AChR subunit genes. We show that all the ten mutations in *COLQ*, *CHRND*, and *CHRNE* in Japanese patients are ethnically unique, which indicates that most CMS mutations arose *de novo* in recent human history or in each family.

2. Materials and methods

2.1. Ethical approval

All the human studies were approved by the institutional review boards of Nagoya University Graduate School of Medicine, Mayo Clinic, Segawa Neurological Clinic for Children, Nagoya City University, and Tokyo Women's Medical University. Appropriate written informed consent was obtained from all the patients and family members.

2.2. Mutation analysis and splicing analysis

Genomic DNA was isolated from peripheral blood with QIAamp Blood Kit (QIAGEN). We directly sequenced all exons with their flanking noncoding regions of *CHRNE*, *CHRNA1*, *CHRNB1*, and *CHRND* in this order with CEQ 8000 (Beckman Coulter). To look for large-scale DNA rearrangements in patient (Pt.) 4, we performed mate-pair sequencing of the whole genome using SOLiD4 (Life Technologies). The mate-pair library was made to span ~2 kb genomic segments according to the manufacturer's protocols. A total of 14.9 Gb of reads were mapped to human genome GRCh37/hg19 with the mapping efficiency of 89% using CLC Genomics Workbench (CLC Bio). All the reads mapped to *CHRNE* were visually scrutinized using Integrative Genome Browser (Broad Institute). Total RNA was isolated from biopsied muscle that was obtained for histopathological diagnostic purposes using RNeasy mini kit (QIAGEN). cDNA was synthesized with ReverTra Ace (Toyobo) and Oligo(dT) Primer (Life Technologies).

2.3. Expression of AChR subunit genes in HEK293 cells

Human α, β, δ, and ε subunit cDNAs were cloned into the CMV-based vector pRBG4 for expression in HEK293 cells [13]. The identified mutations were engineered into wild-type AChR subunit cDNAs in pRBG4 using the QuikChange site-directed mutagenesis kit (Stratagene). Presence of each mutation and absence of unwanted artifacts were confirmed by sequencing the entire inserts. HEK293 cells were transfected with pRBG4-α, -β, -δ, -ε, and pcDNA3.1-EGFP at a ratio of 2:1:1:1:1 using FuGENE 6 transfection reagent (Promega). After 48 hrs, cells were incubated with α-bungarotoxin Alexa Flour 647 (Life Technologies) (1:200) in PBS for 1 hr. Signals were observed under an Olympus BX60 fluorescence microscope. The cells were trypsinized, washed with PBS, and resuspended in PBS. The total number of α-bungarotoxin-binding sites on the cell surface and EGFP was determined by the FACSCalibur system (BD Biosciences).

2.4. Single channel recordings

HEK293 cells were transfected with pRBG4-α, -β, -δ, and -ε, and pEGFP-N1 at a ratio of 2:1:1:1:1, using FuGENE 6. Recordings were obtained at 24 hrs after transfection in the cell-attached configuration at a membrane potential of –80 mV at 22 °C and with bath and pipette solutions containing (in mM): KCl, 142; NaCl, 5.4; CaCl2, 1.8; MgCl2, 1.7; HEPES, 10, pH 7.4. Single-channel currents were recorded using an Axopatch 200B amplifier (Axon Instruments) at a bandwidth of 50 kHz, digitized at 5-μs intervals using Digidata 1322A (Axon Instruments) and recorded to a hard disk using the program Clampex 8.2 (Axon Instruments). Recordings obtained with ACh at 1 μM or less were analyzed at a uniform bandwidth of 10–11.7 kHz with dead time of 15.3–17.9 μs imposed. Recordings obtained with ACh at 10 μM or more were analyzed with dead time at 25 μs at 10 kHz with TAC software (Ver. x4.0.9, Bruxton). Dwell-time histograms were plotted on a logarithmic abscissa and fitted by the sum of exponentials by maximum likelihood, as previously reported [14].

3. Results

3.1. Clinical features

All Pts. had an abnormal decremental response to repetitive nerve stimulation, and no anti-AChR and anti-MuSK antibodies. Clinical features and repetitive nerve stimulation results are summarized in Table 1.

Pt. 1 (13 y.o., male) had eyelid ptosis since age six months and a positive edrophonium test. Clinical features were previously reported in a local journal [15]. Steroid pulse therapy at ages four and five years and thymectomy at age six years had no effect. Combined use of distigmine 3 mg/day and pyridostigmine 180 mg/day enabled him to sit in a chair without assistance at age 13 years. Biopsy of deltoid muscle at age eleven years showed marked AChR deficiency by fluorescent staining with α-bungarotoxin and simplified endplates by electron microscopy.

Pt. 2 (26 y.o., female) had nasal obstruction since birth and eyelid ptosis since age one month. She had a positive edrophonium test and was thought to have myasthenia gravis. Cholinesterase inhibitors were mildly effective. She has ophthamoparesis, and is able to walk but is unable to run.

Table 1
Clinical features of six patients.

Pt.	Sex	Age	Onset	Consanguinity	Repetitive N. stimulation[a]	Drug[b]
1	M	13 y	6 m	–	Accessory N., 60%; Ulnar N., 53%	Distigmine 3 mg + pyridostigmine 180 mg, effective; 3,4-DAP 40 mg, mildly effective
2	F	26 y	1 m	+	Ulnar N., 80%	Pyridostigmine 150–180 mg, mildly effective
3	F	38 y	1 y	–	Ulnar N., 81%	Pyridostigmine 90–160 mg, moderately effective
4	F	6 y	2 y	–	Median N., 60%; Ulnar N., 68%	Pyridostigmine 90 mg + 3,4-DAP 30 mg, mildly effective; ephedrine 25 mg, effective
5	M	26 y	1 m	+	Ulnar N., 76%	Pyridostigmine 135 mg, moderately effective
6	M	11 y	Birth	–	Median N., 35%; Ulnar N., 31%	Prednisolone 35 mg *dieb. alt.*, effective

[a] Repetitive N. stimulation, repetitive nerve stimulation at 2–3 Hz. Relative amplitudes of the 5th CMAP are indicated. [b] Simultaneous prescription is indicated by "+".

Pt. 3 (38 y.o., female) had ptosis at age one year and was diagnosed to have myasthenia gravis at age seven years. Since then, she has been taking cholinesterase inhibitors and prednisolone, which seemed to help but could not climb steps after age 19 years.

Pt. 4 (6 y.o., female) walked alone at age 18 months, but since age two years she had repeated episodes of generalized muscle weakness that lasted about a week, especially when having a common cold. She could walk alone but was positive for a Gowers' sign. Cholinesterase inhibitors were moderately effective. Neurological examination of the mother detected no abnormality. The father was asymptomatic according to the mother, but was not examined by us. Clinical features were previously reported as patient 4 in a local journal [16].

Pt. 5 (26 y.o., male) had feeding difficulty at age one month and had eyelid ptosis since age five months. He has weak facial muscles and is unable to run. At age seven years, he had generalized muscle weakness during an upper respiratory infection. The edrophonium test was positive.

Pt. 6 (11 y.o., male) had repeated respiratory distress and respiratory infection during infancy. He walked alone at age one year, but was noticed to walk slowly at age five years with frequent falling episodes. Rest for a short time improved his walking, but there was no diurnal fluctuation of the symptoms. Intravenous administration of edrophonium chloride ameliorated walking difficulty, but long-acting cholinesterase inhibitors had no effect.

3.2. Mutation analysis

We directly sequenced AChR subunit genes in Pts. 1–6, and identified six mutations in *CHRND* and *CHRNE*, as well as a polymorphism in *CHRNB1* (Table 2). In this study, approved nucleotide and amino acid positions are used instead of the legacy annotation, in which nucleotide and amino acid positions start from the initiation sites of mature peptides.

Pt. 1 was compound heterozygous for c.1372-1G>A at the 3′ end of intron 11 of *CHRND* and c.127C>T predicting p.Arg44Trp at the extracellular domain of the δ subunit (Fig. 1A). cDNA extracted from biopsied muscle revealed that a newly generated 'ag' dinucleotide that was one nucleotide downstream of the native 'ag' was used as a splice acceptor site (Fig. 1B), which predicted p.Glu458Argfs*20 in the long cytoplasmic loop of the δ subunit (Fig. 1A). Pt. 2 was homozygous for c.655_665del predicting p.Gly219Argfs*7 in the extracellular domain of the ε subunit (Fig. 1A). Pt. 3 was heterozygous for p.Tyr262Ter in the M1 transmembrane domain of the ε subunit (Fig. 1A). Pt. 4 was heterozygous for p.Thr284Pro in the M2 transmembrane domain of the ε subunit (Fig. 1A). Pt. 5 was homozygous for p.Leu304Arg in the short extracellular link between the M2 and M3 transmembrane domains of the ε subunit (Fig. 1A). Pt. 6 was heterozygous for p.Met465Thr close to the C-terminal end of the long cytoplasmic loop connecting the M3 and M4 transmembrane domains of AChR β subunit (Fig. 1A).

Table 2
Six mutations and one polymorphism identified in AChR subunit genes.

Pt.	Gene	Nucleotide change[c]	Amino-acid change[c]	Legacy annotation[d]	Phenotypic consequence
1	*CHRND*	c.1372-1G>A	δp.Glu458Argfs*20	δE437fs	AChR deficiency
	CHRND	c.127C>T	δp.Arg44Trp	δR23W	AChR deficiency
2[a]	*CHRNE*	c.655_665del	εp.Gly219Argfs*7	εG199fs	AChR deficiency
3[b]	*CHRNE*	c.786C>G	εp.Tyr262Ter	εY242X	AChR deficiency
4	*CHRNE*	c.850A>C	εp.Thr284Pro	εT264P	SCCMS
5[a]	*CHRNE*	c.911T>G	εp.Leu304Arg	εL284R	AChR deficiency
6	*CHRNB1*	c.1394T>C	εp.Met465Thr	βM442T	~50% shortening of AChR openings

[a] Patient is homozygous for the mutation.
[b] A mutation on another allele remains unidentified.
[c] Nucleotide and amino acid positions start from the translational start sites.
[d] In legacy annotation, nucleotide and amino acid positions start from the initiation sites of mature peptides, which are 69 nt. (23 amino acids), 63 nt. (21 amino acids), and 60 nt. (20 amino acids) downstream of the translational start sites of *CHRNB1*, *CHRND*, and *CHRNE*, respectively.

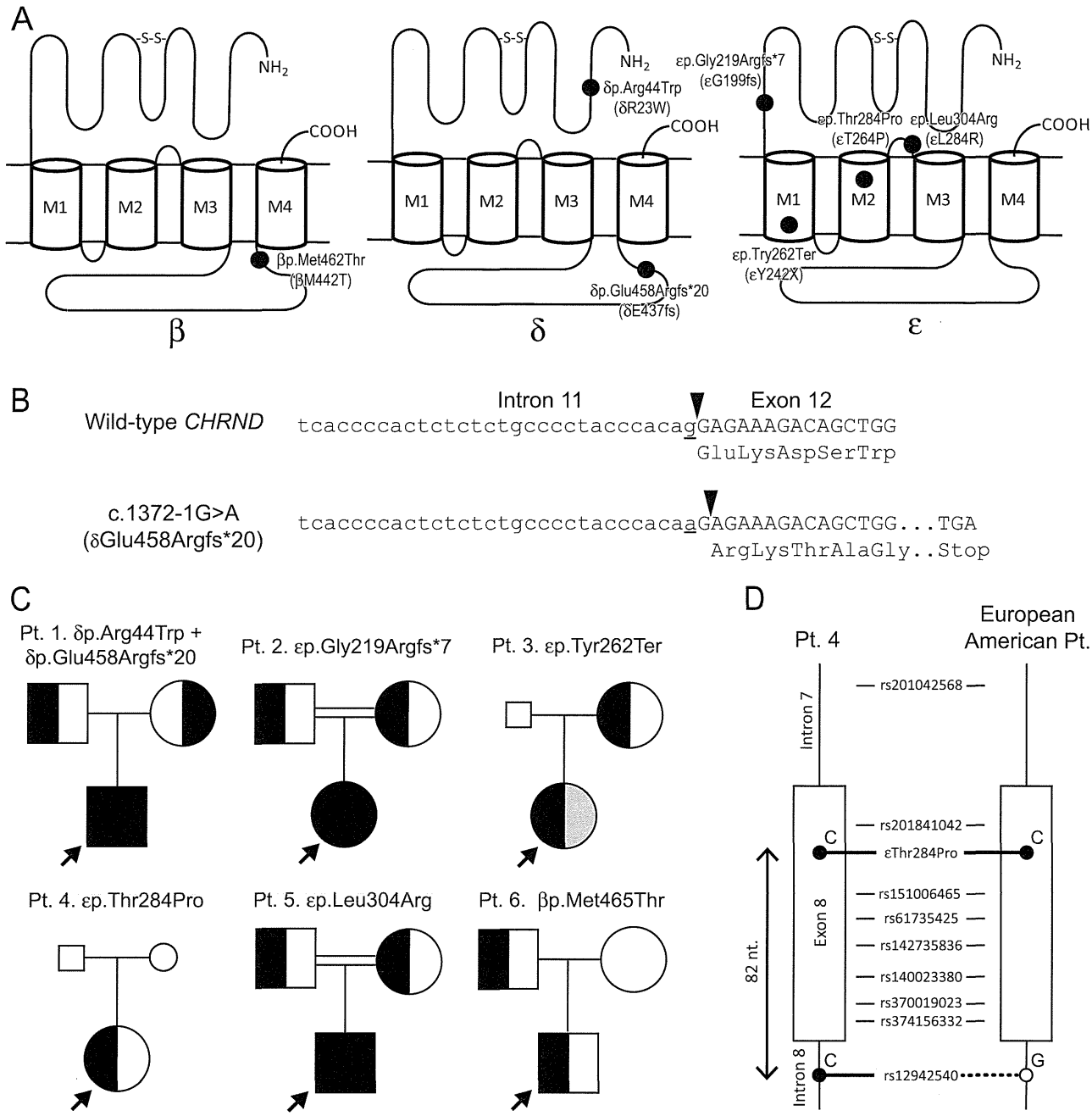

Fig. 1. Six mutations and a single polymorphism in AChR subunit genes identified in six CMS patients. (A) Positions of six mutations and a polymorphism. M1-M4, the first to fourth transmembrane domains. The M2 domains form a channel pore of AChR. (B) RT-PCR of biopsied muscle of Pt. 1 reveals that c.1372-1G>A (underlined) shifts a splice acceptor site (arrowheads) one nucleotide downstream, which predicts a shift in the reading frame (δp.Glu458Argfs*20). (C) Pedigree analyses of the mutations. Patients are indicated by arrows. Full and half shaded symbols represent homozygous and heterozygous mutations, respectively. Gray half shaded symbols represent that the individuals are predicted to carry a heterozygous mutation, the identity of which, however, has not been identified. Small symbols indicate that DNA is not available. (D) Haplotype analysis of εp.Thr284Pro in Pt. 4 and the previously reported European American Pt [7]. Both patients carry discordant nucleotides at rs12942540, which is 82 nt. downstream of the mutation.

δp.Arg44Trp (rs55868108) in Pt. 1 was previously reported in one of five healthy controls, but its ethnic origin was not documented [17]. δp.Arg44Trp, however, is not observed in the 1000 genome project (http://www.1000genomes.org/) or in the human gene variation database (HGVD), which collates SNPs in a large cohort of Japanese individuals (http://www.genome.med.kyoto-u.ac.jp/SnpDB/) [18]. As indicated below, functional analysis disclosed that δp.Arg44Trp

Table 3
Open intervals and bursts of wild-type and mutant AChR expressed on HEK cells.

	Open intervals		Bursts	
	Wild-type	βp.Met465Thr	Wild-type	βp.Met465Thr
τ_1 (ms)	0.037 ± 0.0033[a]	0.022[b]	0.036 ± 0.0017[c]	0.039 ± 0.006[d]
(a_1)	(0.17 ± 0.022)	(0.18)	(0.24 ± 0.021)	(0.18 ± 0.034)
τ_2 (ms)	0.31 ± 0.050	0.16 ± 0.017[e]	0.47 ± 0.059	0.16 ± 0.037[f]
(a_2)	(0.27 ± 0.038)	(0.23 ± 0.031)	(0.21 ± 0.027)	(0.23 ± 0.010)
τ_3 (ms)	1.35 ± 0.051	0.98 ± 0.034	3.31 ± 0.12	1.93 ± 0.085
(a_3)	(0.67 ± 0.042)	(0.78 ± 0.028)	(0.58 ± 0.038)	(0.82 ± 0.034)

Twenty-one wild-type and seven mutant patches were analyzed. Time constants, τ_n, and fractional areas, a_n, for each component are presented with mean ± SEM. ACh concentration was 50–100 nM.
[a–f] Not detected at 12, 6, 3, 5, 1, and 3 patches, respectively.
Final band widths were 11.7 and 10 kHz for wild-type and mutant AChRs, respectively.

significantly reduces cell surface expression of AChR and is unlikely to be polymorphism.

p.Met465Thr (rs201776800) in Pt. 6 was observed in eight alleles in eight Japanese individuals in the 1000 genome project with a minor allelic frequency (MAF) of 0.004, as well as in 119 alleles in a cohort of 1170 Japanese individuals in HGVD with a MAF of 0.051. Although p.Met465Thr was likely to be a polymorphism according to the high MAFs in the Japanese, we scrutinized functional consequences of p.Met465Thr in this study.

*3.3. εp.Gly219Argfs*7, εp.Tyr262Ter, and δp.Glu458Argfs*20 are predicted to compromise AChR expression*

Among the six mutations, εp.Gly219Argfs*7 in Pt. 2 and εp.Tyr262Ter in Pt. 3 were predicted to produce truncated ε subunits. We previously reported that truncation mutations in the εsubunit lead to expression of the embryonic $\alpha_2\beta\delta\gamma$-AChR at the patient's endplates and the patients have endplate AChR deficiency [19–21]. The ε mutations in Pts. 2 and 3 were thus predicted to cause AChR deficiency.

δp.Glu458Argfs*20 in Pt. 1 was predicted to generate a truncated δ subunit that cannot be incorporated into mature AChR. The phenotype of Pt. 1 is thus determined by δp.Arg44Trp on the other allele, which causes AChR deficiency as indicated below.

3.4. εp.Thr284Pro is an established slow-channel mutation without shared haplotype with a European American patient

εp.Thr284Pro in the M2 domain of the ε subunit was identical to the first characterized slow-channel mutation reported in a patient of Swiss and Turkish descent [22]. We asked if the mutation in Pt. 4 derived from the same founder allele as the first reported patient. Therefore we sequenced exon 8 and its flanking intronic regions where nine SNPs were located (Fig. 1C). This revealed that the mutant allele in the Japanese patient had 'C', whereas the mutant allele in the European American patient had 'G' at rs12942540 in intron 8, which was located 82 nt. downstream of εp.Thr284Pro. Accordingly, εp.Thr284Pro in both patients is likely to have occurred independently in two ethnic groups.

3.5. δp.Arg44Trp and εp.Leu304Arg, but not βp.Met465Thr, decrease cell surface expression of AChR in transfected HEK293 cells

We next analyzed the effects of AChR expression of the remaining three mutations of δp.Arg44Trp, εp.Leu304Arg and βp.Met465Thr. We introduced wild-type or mutant α, β, δ, and ε subunit cDNAs along with EGFP cDNA into HEK293 cells (Fig. 2A), and measured cell surface expression of AChR detected by Alexa 647-labeled α-bungarotoxin using FACS. Expression of βp.Met465Thr-AChR was similar to that of wild-type AChR, whereas δp.Arg44Trp and εp.Leu304Arg markedly attenuated the cell surface expression of AChR (Figs. 2B and C). Accordingly, δp.Arg44Trp and εp.Leu304Arg cause endplate AChR deficiency.

3.6. βp.Met465Thr mildly shortens channel opening events, but not as much as the other established fast channel mutations

As βp.Met465Thr-AChR was efficiently expressed on HEK293 cells, we next recorded opening and closing of single AChR channels at limiting low concentrations of ACh by the patch clamp method (Fig. 3A). We found that the major burst duration (τ_3) was decreased from 3.31 ms to 1.93 ms (58.3%) in βp.Met465Thr-AChR (Table 3), while the conductance of βp.Met465Thr-AChR was normal. Distributions of opening probabilities of the clusters generated by 10 μM or greater concentrations of ACh made single peaks for both wild-type and mutant AChRs. Thus, βMet465Thr mildly shortens the channel openings but does not cause a mode switching in the kinetics of the receptor activation, which is seen in other FCCMS mutations [23,24].

3.7. A recessive mutation on the other allele in Pt. 3 remains unidentified

Functional prediction and characterization of the six mutations indicated that εp.Thr284Pro in Pt. 4 was a dominant slow-channel mutation [22], whereas the other five mutations in Pts. 1, 2, 3, and 5 were recessive loss-of-function mutations. The mutations in Pts. 1, 2, and 5 were biallelic, whereas a mutation was detected only on a single allele in Pt. 3 (Fig. 1C).

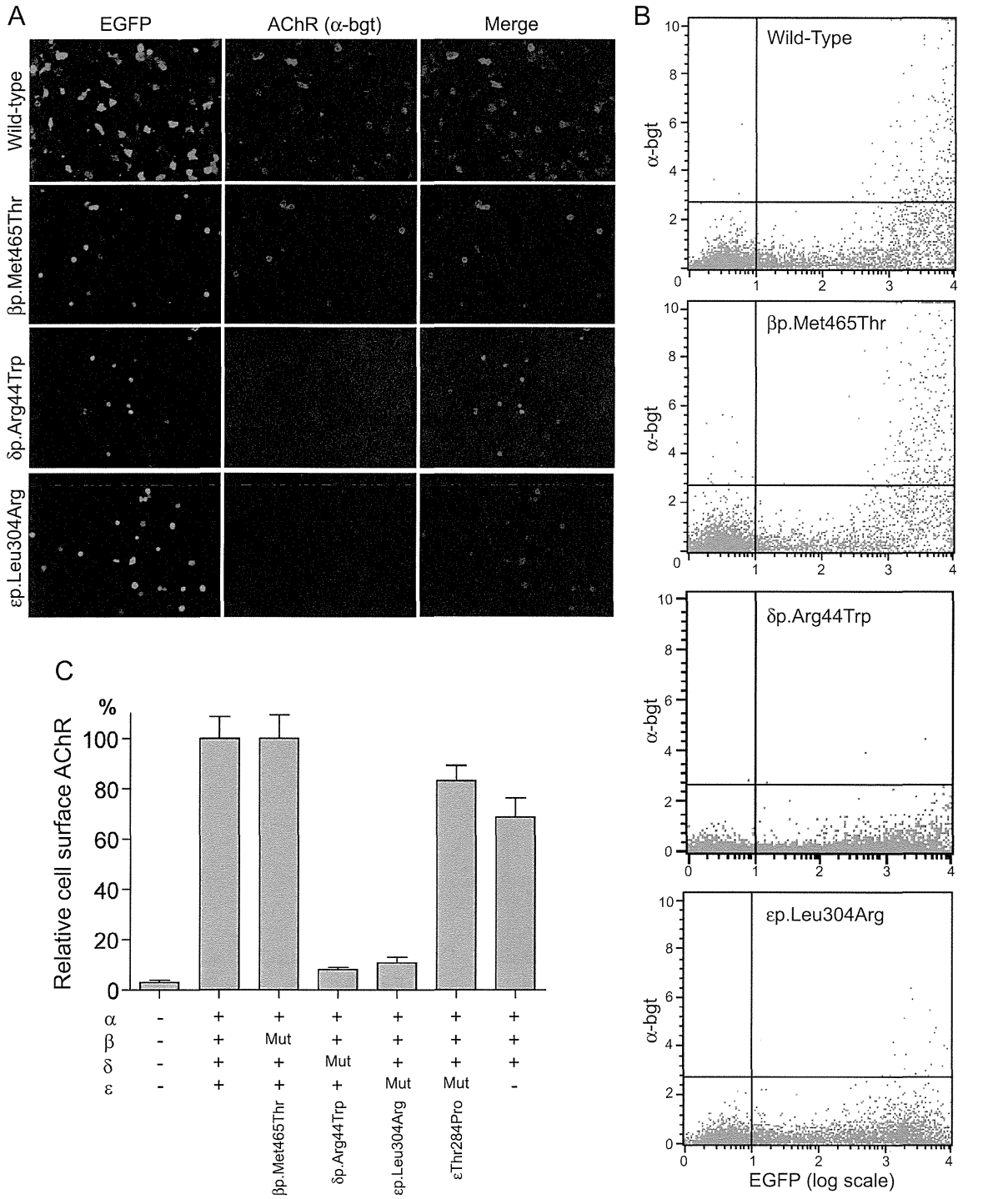

Fig. 2. Quantification of cell surface expression of wild-type and mutant AChRs on HEK293 cells. (A) HEK293 cells are transfected with wild-type or mutant AChR subunit cDNAs along with EGFP cDNA. Only transfected cells have EGFP signals and AChRs that are visualized with Alexa 647-labeled α-bungarotoxin (bgt). εp.Leu304Arg-AChR has less signals for AChRs compared to wild-type and βp.Met465Thr-AChRs. (B) Representative FACS profiles of EGFP and Alexa 647-labeled α-bgt. Both axes are shown in arbitrary units. The number of cells fractioned into the upper right quadrant is counted as AChR-positive cells. (C) Ratios of AChR-positive cells (the upper right quadrant) divided by EGFP-positive cells (the lower right quadrant). δp.Arg44Trp and εp.Leu304Arg markedly decrease AChR expression, whereas βp.Met465Thr and εp.Thr284Pro have no effect on AChR expression. ε-deficient $\alpha_2\beta\delta_2$-AChR are expressed at ~70% of wild-type, as we reported previously [21]. Mut, a mutant AChR subunit. Mean and SE are indicated ($n = 12$).

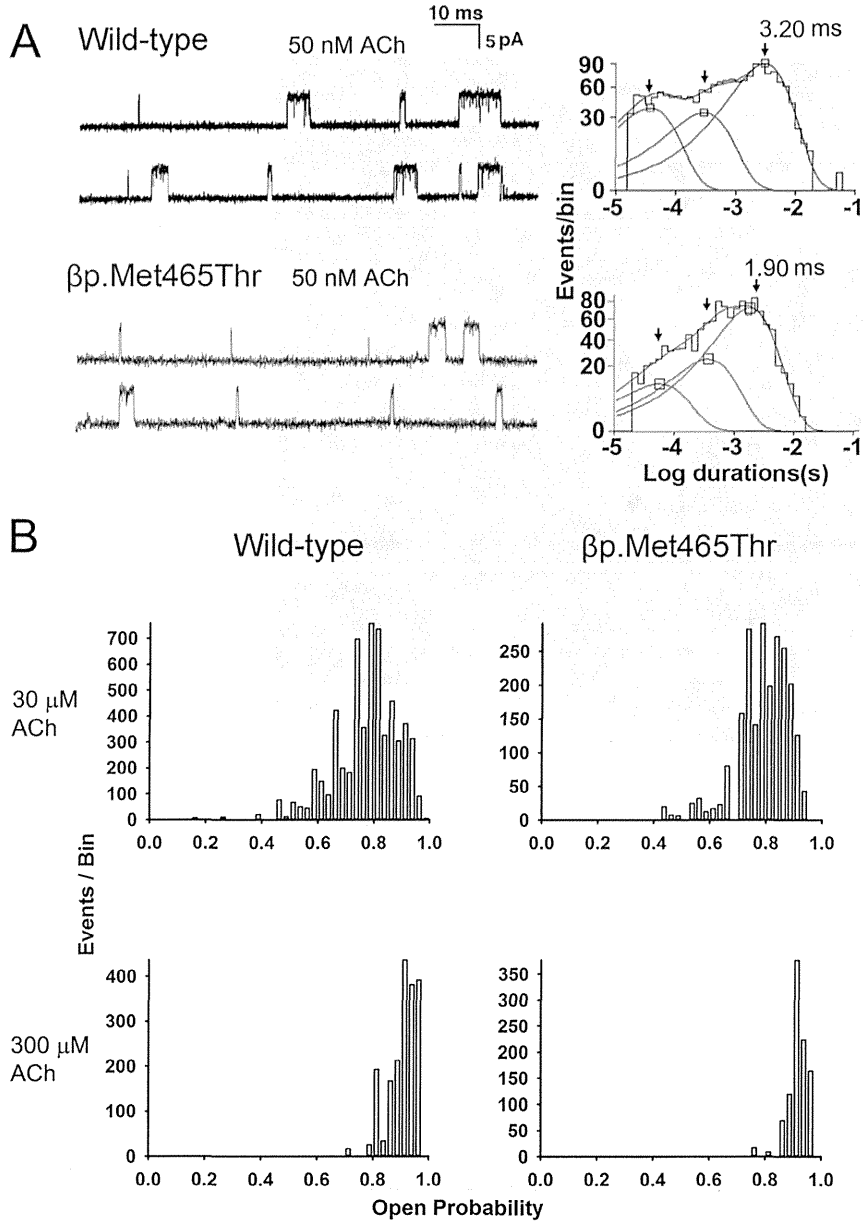

Fig. 3. Single channel currents of wild-type and mutant AChRs on HEK293 cells. (A) Left: Representative channel openings shown as upward deflections. Right: Burst duration histograms fitted to the sum of exponentials. Arrows indicate mean durations of dominant burst components. (B) Distribution of open probabilities from individual clusters obtained at the indicated ACh concentrations. Note that both wild-type and mutant AChRs make a single peak.

We scrutinized all exonic nucleotides in *CHRNE* in Pt. 3 by bidirectional sequencing, but detected none. We therefore hypothesized that a mutation on the other alleles was either a promoter mutation, a splice-site mutation disrupting a deep intronic splicing *cis*-element, or a large-scale DNA rearrangement. Sequencing of ~1 kb upstream of the translation initiation sites, however, revealed no mutation. We further analyzed genomic DNA by mate-pair sequencing of the whole genome. A total of 57 reads were mapped to *CHRNE*. Visual inspection of these reads, however, failed to detect any large-scale DNA rearrangements or any mutations. A recessive mutation on the other allele in *CHRNE* in Pt. 3 thus remains unidentified. We also analyzed 18 other CMS-causing genes using the mate-pair sequencing data in Pt. 3. As the mate-pair sequencing was for detecting a large-scale DNA rearrangement, the 18 genes were covered by only 10,116 reads. Although the coverage was not high enough for detecting SNVs, no candidate mutations were detected in Pt. 3.

Table 4
Fifteen previously reported FCCMS mutations and the currently analyzed βp.Met462Thr polymorphism.

Mutation	Burst duration (ms)			Expression	Domain	Reference
	Wild-type	Mutant	Ratio	(%)		
αp.Val152Leu (αV132L)	3.31	0.50	0.151	135	Extracellular domain of α	[25]
αp.Val208Met (αV188M)	3.31	0.68	0.205	90	Extracellular domain of α	[26]
αp.Phe276Leu (αF256L)	3.62	0.30	0.083	102	M2 domain of α	[27]
αp.Val305Ile (αV285I)	2.99	0.34	0.114	116	M3 domain of α	[28]
δp.Leu63Pro (δL42P)	3.31	0.18	0.054	37	Extracellular domain of δ	[14]
δp.Glu80Lys (δE59K)	5.06	2.75	0.543	62	Extracellular domain of δ	[29]
δp.Pro271Gln (δP250Q)	3.31	1.54	0.465	60	M1 domain of δ	[30]
εp.Thr58Lys (εT38K)	5.86	0.06	0.010	78	Extracellular domain of ε	[31]
εp.Trp75Arg (εW55R)	3.31	0.37	0.112	86	Extracellular domain of ε	[32]
εp.Pro141Leu (εP121L)	2.99	0.45	0.151	102	Extracellular domain of ε	[13]
εp.Asp195Asn (εD175N)	2.13	0.49	0.230	117[b]	Extracellular domain of ε	[33]
εp.Asn202Tyr (εN182Y)	2.13	0.65	0.305	117[b]	Extracellular domain of ε	[33]
εp.Ser433_Glu438dup (ε1254ins18)	2.80	1.01	0.361	47	Long cytoplasmic loop of ε	[23]
εp.Ala431Pro (εA411P)	n.a.[a]	n.a.[a]	n.a.[a]	31	Long cytoplasmic loop of ε	[24]
εp.Asn456del (εN436del)	3.31	1.24	0.375	51	Long cytoplasmic loop of ε	[34]
βp.Met462Thr (βM442T)	3.31	1.93	0.583	99	Long cytoplasmic loop of β	Current study

A major component of burst durations of wild-type and mutant AChRs expressed in HEK293 cells is indicated. Cell surface expression in HEK293 cells is normalized to that of wild-type. Channel openings are elicited by 50–100 nM ACh. Mutations in parentheses are legacy annotations used in original reports.

[a] Detailed ion channel kinetics are analyzed using a hidden Markov model, but burst durations are not indicated.

[b] Cell surface expression of recombinant AChR is not indicated, and the expression ratio is calculated from α-bungarotoxin binding sites of control and patient endplates.

4. Discussion

We identified six mutations in AChR subunit genes in five Japanese patients with CMS. We initially assumed that βp.Met465Thr in Pt. 6 was a mild fast-channel mutation. However, expansion of the SNP database later disclosed that βp.Met465Thr is a polymorphism that is frequently observed in the Japanese population. Fifteen previously reported FCCMS mutations shorten burst durations to 22.6 ± 16.1% of wild-type (mean and SD; range 1.0%–54.3%) (Table 4). A FCCMS mutation, δp.Glu80Lys (δE59K), decreases burst durations to 54.3% of wild-type [29], which is similar to 58.3% observed in the current βp.Met465Thr polymorphism. However, in contrast to βp.Met465Thr, δp.Glu80Lys reduces cell surface expression of AChR to 62% of wild-type [29]. Similarly, δp.Pro271Gln (δP250Q) mildly reduces burst durations to 46.5% of wild-type, but again, unlike βp.Met465Thr, this mutation reduces cell surface expression of AChR to 60% of wild-type [30]. A plot of normalized burst durations and normalized cell surface expressions suggests that a mean burst duration of less than ~30% causes FCCMS even when it does not affect the cell surface expression of AChR (Fig. 4). In contrast, a mean burst duration of between ~30% and ~60% causes FCCMS when the mutation reduces the cell surface expression of AChR to ~60% or less (Fig. 4). However, as no individual is homozygous for βp.Met465Thr or carries a null mutation on the other allele, pathogenicity of βp.Met465Thr in the absence of a normal *CHRND* on the other allele still remains unknown.

δp.Arg44Trp is close to the N-terminal end of the extracellular region (Fig. 5). We previously reported that a similar εp.Arg40Trp also causes AChR deficiency [35]. The specific function of this region, however, is not well dissected. εp.Leu304Arg is in the short extracellular link between the M2 and M3 transmembrane domains (Fig. 5). The functions of this link are not well characterized. In this link, only αp.Ser289Ile (αS269I) is reported in SCCMS [38]. βp.Met465Thr is located close to the C-terminal end of the long cytoplasmic loop that links the M3 and M4 transmembrane domains (Fig. 5). Interestingly, three FCCMS mutations in the long cytoplasmic loop are clustered close to the C-terminal end of the ε subunit [23,24,34,36,37], and similarly destabilize the channel open state. Two FCCMS mutations in this region, εp.Ser433_Glu438dup (ε1254ins18) [23] and εp.Ala431Pro (εA411P) [24], disrupt the fidelity of gating and result in unstable channel kinetics. In addition, another FCCMS

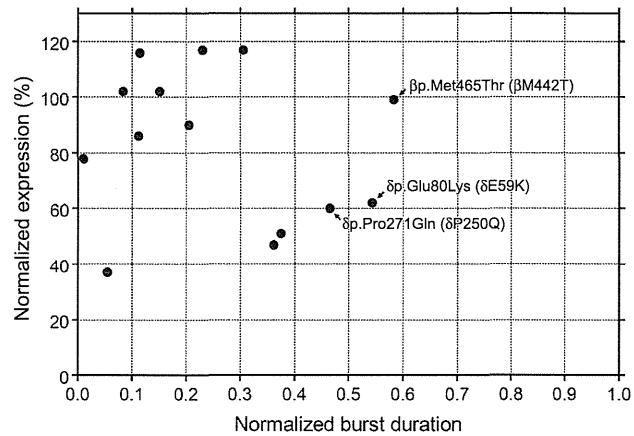

Fig. 4. Normalized burst durations and normalized cell surface expressions of previously reported FCCMS mutations and the currently analyzed βp.Met462Thr polymorphism shown in Table 4. Arrows point to mutations and a polymorphism that are addressed in the discussion.